AD-A064 314 AIR FORCE INST OF TECH WRIGHT-PATTERSON AFB OHIO SCH--ETC F/G 20/5
BEAM PROFILING OF A MULTIMODE LASER.(U)
DEC 78 R J LICATA

UNCLASSIFIED AFIT/GEP/PH/78D-7 NL

1 OF 1
AD A064 314

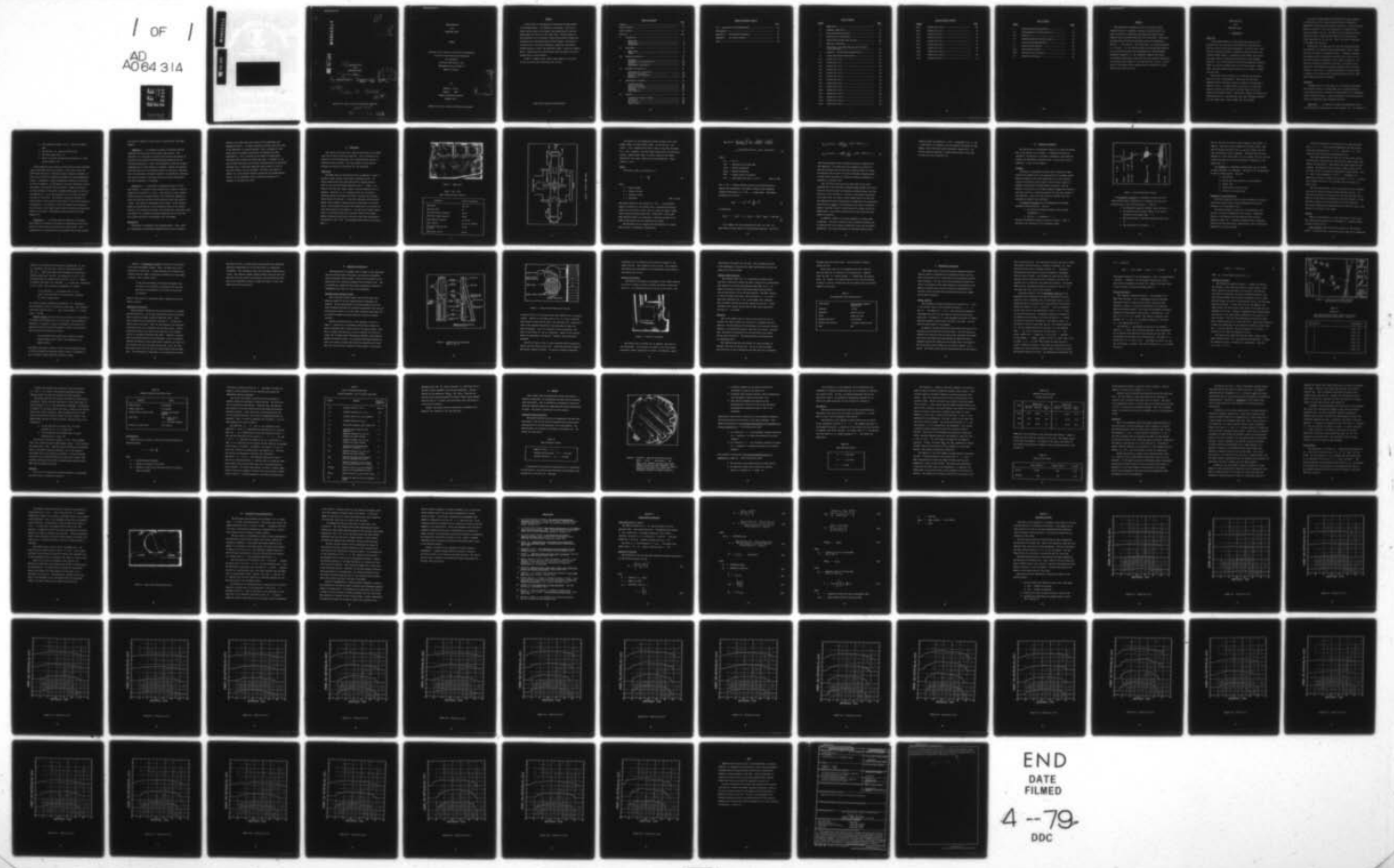

END
DATE FILMED
4 -79
DDC

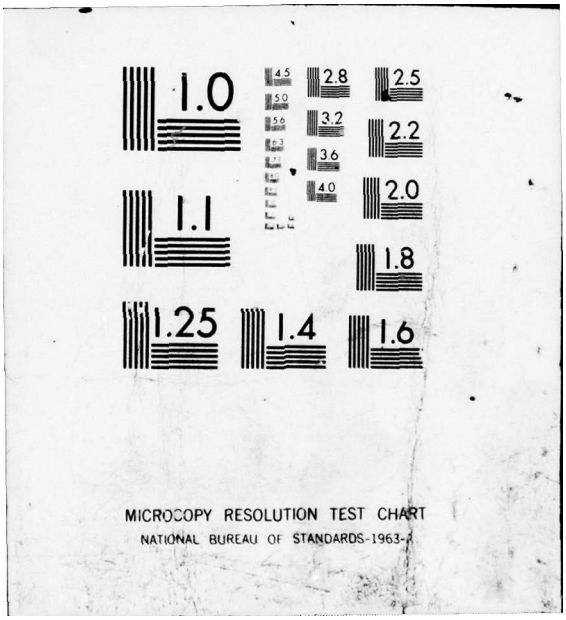
1.0
1.1
1.25
1.4
1.6
1.8
2.0
2.2
2.5
2.8
3.2
3.6
4.0
4.5
5.0
5.6
6.3
MICROCOPY RESOLUTION TEST CHART
NATIONAL BUREAU OF STANDARDS-1963-A

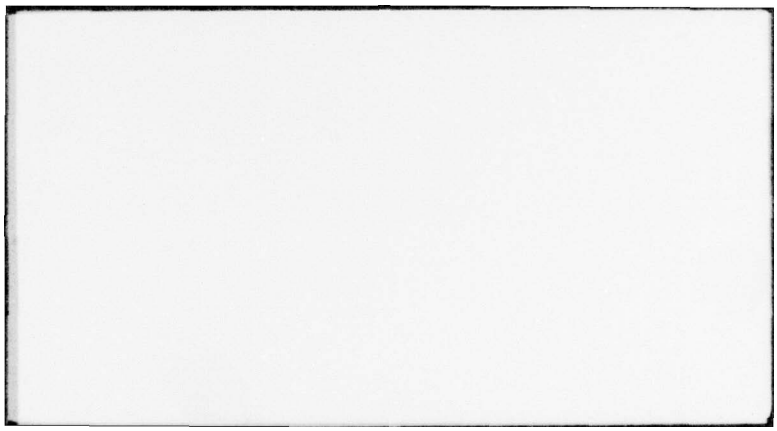

AFIT/GEP/PH/78D-7

(1)

LEVEL II

AD A064314

DDC FILE COPY

(6) BEAM PROFILING
OF A
MULTIMODE LASER.

(9) Master's THESIS,

(14) AFIT/GEP/PH/78D-7

(10) Raymond J. Licata
Captain USAF

DDC
RECEIVED
FEB 8 1979
A

(12) 92p.

(11) Dec 78

(16) 1736D

(17) $2

Approved for public release; distribution unlimited.

012 225

79 01 30 109

AFIT/GEP/PH/78D-7

BEAM PROFILING
OF A
MULTIMODE LASER

THESIS

Presented to the Faculty of the School of Engineering

of the Air Force Institute of Technology

Air University

in Partial Fulfillment of the

Requirements for the Degree of

Master of Science

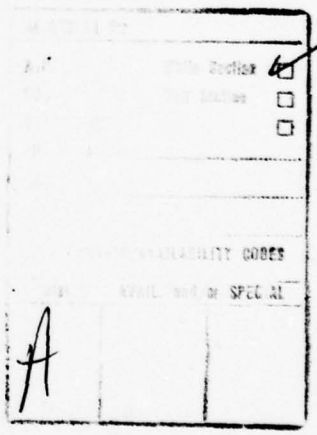

by

Raymond J. Licata

Captain USAF

Graduate Engineering Physics

December 1978

Preface

In this effort to experimentally investigate the beam profile of a multimode laser, I am indebted to many people. First is my thesis advisor, Major Glenn Doughty, who enthusiastically gave me needed advice and kept me on the right track. Special thanks are also extended to Dr. Ed Rolinski, without whose positive support and cooperation this experiment would not have existed. Then there is the whole crew at the Acurex Laboratory, especially John Bagford and Dale Hurley, to whom I owe particular thanks. During the computer phase, I leaned heavily on Rick Schuster and Dave McGrew, who saved me many weeks in data reduction.

Finally, I thank my wife, without whose support in all areas of our lives this effort would have been in vain.

(This thesis typed by Sharon Gabriel)

Table of Contents

Table of Contents (Cont'd)

List of Figures

List of Figures (Cont'd)

List of Tables

Abstract

The experimental investigation into the intensity profile characteristics of a multimode, high-power, continuous-wave, CO_2 laser is presented. Quantitative one-dimensional profiles were obtained using an enhanced swept null point calorimeter. Qualitative two-dimensional profiles were obtained using the IR transparency material -- 3M, Type 577. The results were: (1) the beam divergence is 3.75 mrad ; (2) the intensity profile is characterized basically by a circular mode pattern, but superimposed by a distinguishable rectangular component; (3) the rectangular component only varies in intensity proportional to the laser power and inversely proportional to the optical path length; (4) the shot stability is about ± 7 w/cm^2 ; and, (5) the average profile deviation from an idealized "flat top" profile varies from 11 to 15%.

BEAM PROFILING

OF A

MULTIMODE LASER

I. Introduction

Motivation

It has become apparent in recent years that the era of the multikilowatt laser has arrived with significant applications to both the civilian and military environment. In the Air Force, there has been a significant effort to develop the high power laser into effective weapon systems. In addition to this effort, there exists the counter effort to develop laser resistant or laser hardened materials. One of the missions of the Air Force Materials Laboratory (AFML) is to do this counter effort for Air Force systems. Specifically, the Laser Hardened Materials Branch (LPJ) of AFML is charged with this work.

Since laser material response is a relatively new phenomenon, much of the work is experimental. Toward this end, the Laser Hardened Materials Evaluation Laboratory (LHMEL) was established in AFML/LPJ in 1976. The LHMEL provides facilities to all bona fide users for controlled irradiation of specimen targets at the 10.6 microns (μm) wavelength region. They employ a nominal 10 kilowatt (kw), continuous-wave (cw), carbon-dioxide (CO_2) laser (hereafter referred to as the LHMEL laser, or more simply, just as the laser).

As an aid to understanding the mechanism of material responses, it is desirable to have a beam intensity profile as azimuthally symmetrical, uniform and time-invariant as possible. Such an idealized profile is known as a "flat top" because the 2-D intensity cross section resembles a top hat. The LHMEL laser was designed with this objective in mind. Plexiglass burns made by the laser indicate a "good" approximation to a flat top. Thus, this laser is identified as the LHMEL flat top laser.

Nevertheless, the LHMEL beam has never been carefully defined and invariably, the material response experimenters tend to "blame" the laser for unusual or unexpected results. Attempts at improving the present profile are hindered since there are no clear cut facts as to what laboratory parameters, if any, affect the profile. The materials response of plexiglass reacts only to relatively gross variations. Some parameters are easily adjustable from a practical viewpoint. Many are not. No further expenditures of time or money to improve the beam quality were considered appropriate until these basic difficulties could be resolved.

Objectives

The main objective of this thesis is to empirically investigate the intensity profile of the AFML/LHMEL laser, thereby determining if the extent of profile variations is large enough to be a significant factor in material effects. Toward fulfillment of this main objective, there were established four subsidiary objectives.

Objective A -- to determine the LHMEL beam divergence as well as the qualitative characteristics of the intensity (I) as a function of

1. The transverse distance (x & y) across the optical path
2. The distance (z) along the optical path
3. The laser output power (P)
4. And as a function of power and the presence of a beam splitter/window (SF) .

These parameters were selected as being the most easily adjustable under normal LHMEL operating conditions. Since this facility was established basically to investigate material response phenomena, the laser itself and various supportive equipment have become permanently located. Consequently, certain experimental constraints were placed on various parameters. Establishment of the exact functional relationship between the intensity and the distance or power would require at least knowledge of the number of spatial modes present in the beam (see Chapter II). To do this empirically for this laser was beyond the scope of this effort. Nevertheless, qualitative analysis can yield results as to the overall effectiveness of the factors discussed in Objective A. The selection of the beam splitter was selected as the one element in the normal optical path that may have an appreciable effect on the profile. Experimental evidence supports this (see Chapter III).

Objective B -- to evaluate the shot stability of the laser. Shot stability is defined as the degree of reproducibility from laser firing to laser firing for any given set of input values. This reproducibility is important when the irradiance must be kept constant

in a series of samples or when trying to correlate data from among samples.

Objective C -- to estimate the extent of variation from the idealized flat top profile at the normal test position. Some indication as to the range of variation from the flat top profile at the present test position would differentiate between one of the following possibilities. First, the percentage of variation is found acceptable and no future analysis is required. Second, the variation found indicates that a more precise analysis of the data is advisable. Last, the percentage of variation appears to be significant; therefore, more precise analysis of the data, as well as future investigation into other parameters, is indicated.

Objective D -- to establish an extended data base of valid beam profiles. The amount of data acquired was in excess of what was required for objectives A, B, and C. This was done so that, whenever further analysis was deemed advisable, work could begin immediately using this data base and thus avoid substantial delay (many months to a year). This delay is attributable to two causes. First, frequent delays are encountered due to the inoperative status or the unavailability of the key detection system, the Aerotherm Laser Calorimeter (ALC) (see Chapter IV); secondly, the general unavailability of laser time for in-house work due to the extremely heavy user demand.

Organization

This thesis is organized in the following manner. First, there is a presentation of applicable background material which includes a

section on the LHMEL laser and a section on the applicable beam propagation physics. A formative discussion follows, where the scope of the experiment is carefully defined. Then, in Chapter IV, the major pieces of equipment and material are reviewed with their applicability. This is followed by the chapter on Experimental Procedures which explains how things were done. In Chapter VI, the basic results obtained by the two major detection pieces are presented. Following that, a discussion summarizes these results, as well as any error analysis that was performed. The basic text ends with Chapter VII, which presents specific conclusions and recommendations. Finally, the two appendices contain information important for repeating or extending this work.

II. Background

This chapter will start with a physical description of the LHMEL laser and its basic operating limitations. This is followed by an analysis of the field expression for an individual mode and how it affects the total waveform. This last section, entitled Theory, provides the theoretical motivation for this experiment.

LHMEL Laser

The LHMEL laser was specifically built for AFML/LPJ in order to provide a highly reliable "push button" operational laser. Its design specifications were duplicated from an already operating laser at the Air Force Weapons Laboratory (Ref. 3). Today, it is known as the "flat top" laser; however, strictly speaking, this is a misnomer. Basically, it is a continuous wave (cw) CO_2 electric discharge coaxial laser which uses helium, nitrogen, and obviously, carbon dioxide (see Figure 1). Fast flow techniques utilizing aerodynamic forces produce a uniform electron distribution in the laser cavity. This maximizes the active gain medium which is available for laser mode excitation (see Figure 2). At each end are placed sixteen anodes in an annular array with an annular cathode in the middle. Nominal electrical efficiency is "25% with a mass flow efficiency of 100 kw/lb/sec" (Ref. 3:52). The operating characteristics are given in Table I.

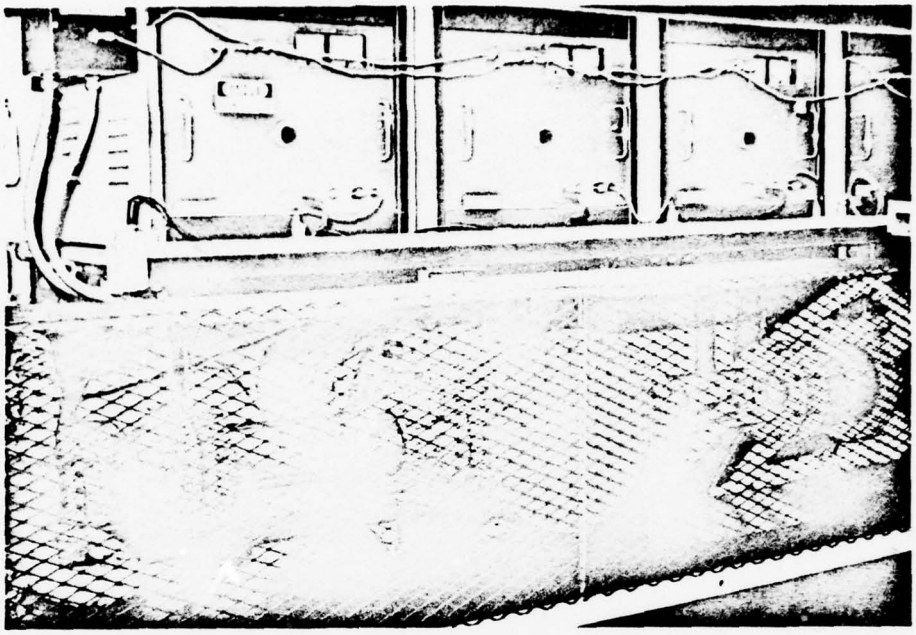

Figure 1. LHMEL Laser

Table I (Ref. 1:19)

Laser Operating Specifications

Parameter	Value of Parameter
Wavelength	10.6 μm
Operating Mode	cw
Max Energy Output (Nominal)	100 KJ
Max Power Output (Nominal)	10 KW
Beam Diameter (Nominal)	1 to 9 cm
Power Density	0.2 to 12.7 KW/cm^2
Max Sample Exposure Time at 10 KW	10 sec
Repeat Rate (80 KJ)	10 min

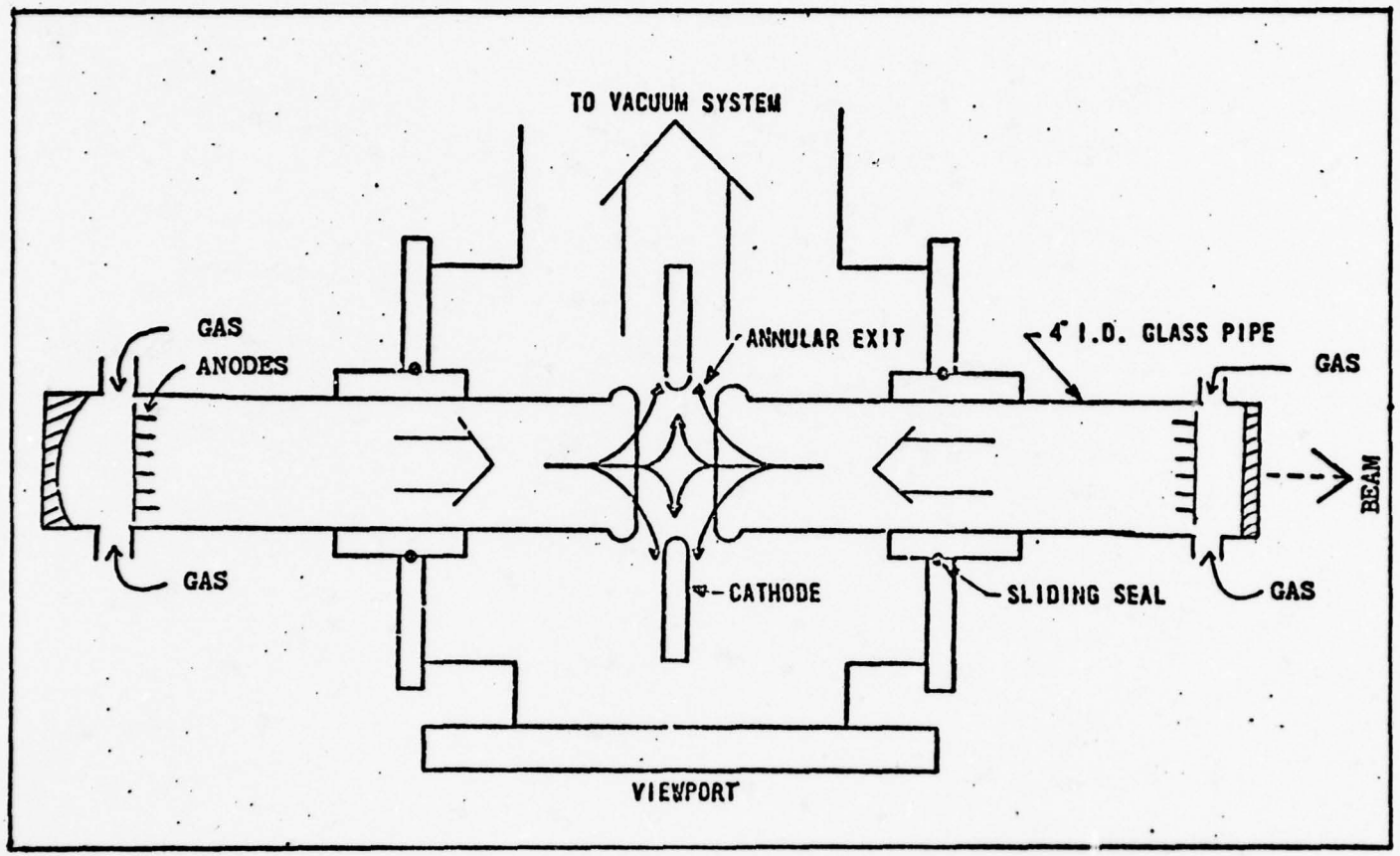

Figure 2. Schmatic LHMEL Laser

The cavity is a half symmetrical stable resonator with a high Fresnel number (low diffraction losses). At one end is a 15 m radius, .114 m diameter Be-Cu mirror, while at the other end there is a .114 m diameter, flat ZnSe output coupler with a 75% reflective coating. Maximum power output is usually limited by the damage threshold of this output coupler due to heat absorption. Cavity length is 2.02 m .

Theory

The Fresnel number, by definition, is

$$N = \frac{a^2}{L\lambda} \tag{1}$$

where

N = Fresnel number

a = radius of mirror

L = resonator length

λ = wavelength (Ref. 11:338)

The Fresnel number for this resonator is 152 . A high Fresnel number is indicative of two things; first, intracavity diffraction losses are very low and, second, that the cavity can support higher order transverse Gaussian modes (Ref. 9:1312-1329). Unless some mode selection scheme is in operation, a laser will operate in all modes simultaneously that the resonator will support.

The expression for the complex field distribution of a single mode is given in rectangular coordinates by

$$\tilde{U}_{mn}(x,y,z) = \left(\frac{2}{2^{m+n}m!n!\pi}\right)^{\frac{1}{2}} \frac{1}{w(z)} H_m\left(\frac{\sqrt{2}x}{w(z)}\right) H_n\left(\frac{\sqrt{2}y}{w(z)}\right)$$

$$x\ e^{-j(k/2)(x^2+y^2)/\tilde{q}(z)}\ e^{-jkz + j(n+m+1)\Psi(z)} \qquad (2)$$

where

m,n = 0,1,2...

$w(z)$ = spot size of 0,0 order mode

x,y,z = spatial coordinates

H_m, H_n = Hermite polynomials

$\tilde{q}(z)$ = complex radius of curvature

$\Psi(z)$ = total phase shift from z = 0 to z (Ref. 11:329)

The m and n indexes identify precisely the transverse mode in question and correspond to the number of nodes in the transverse intensity distribution of x and y , respectively. The Hermite polynomials are given by

$$H_k(x) = (-1)^k\ e^{x^2}\ \frac{\partial^k}{\partial x^k}\ e^{-x^2} \qquad (3)$$

or alternately

$$H_o(x) = 1 \quad H_1(x) = 2x \quad H_2(x) = 4x^2-2 \quad H_3(x) = 8x^3-12x..... \qquad (4)$$

As an example, the exact expressions for the 0,0 and 1,0 order modes are given below for a given spatial position, (x^1,y^1,z^1) .

$$\tilde{U}_{0,0}(x^1,y^1,z^1) = \left(\frac{2}{\pi}\right)^{\frac{1}{2}} \frac{1}{w(z^1)} \; e^{-jkz^1 + j\Psi(z^1)} \; e^{(....)}$$

$$U_{1,0}(x^1,y^1,z^1) = 2\left(\frac{2}{\pi}\right)^{\frac{1}{2}} \frac{x^1}{w^2(z^1)} \; e^{-jkz^1 + j2\Psi(z^1)} \; e^{(....)} \qquad (5)$$

(The final exponential term not explicitly shown is identical for both equations.) The objective of the examples is to point out that the functional form of any single transverse mode will always be different from the form of any other individual transverse mode. In other words, each mode as a function of spatial coordinates is changing at a different rate.

Now, the total wave form of the output beam is the linear superposition of the individual transverse modes present in the beam. Since the individual modes are changing at different rates, the total wave form is also changing as a function of the spatial coordinates. On the other hand, the number of modes present may be so large and the amplitude and phase relationships so complex that the conglomerate beam profile may appear to be unchanging as the spatial coordinates change. Therefore, without actually knowing the number and kind of modes present, even general characteristics of the total wave form cannot be predicted.

In addition, Equation (2) can be expressed in circular polar coordinates. The actual functional form is naturally different and is characterized by the Laguerre polynomials rather than the Hermite polynomials. The intensity patterns of individual modes are also

different where the parameters p and ℓ correspond to the m and n mode numbers in rectangular form and represent the number of nodes present in the radial and angular directions, respectively. For certain resonator geometries, a simpler beam analysis can be made by using this form of Equation (2).

III. Formative Discussion

The first step in an experimental design is to scope the problem. This is the purpose of this chapter. To properly delineate the experiment, the questions of variables, assumptions, approximations, validity and experimental restraints arose. Each of these will be addressed, in turn, in this chapter.

Variables

The number of independent variables that influenced the beam profile were numerous due to the sophistication of the LHMEL system. With the exception of the beam coordinates, all of the variables listed are discussed at great length in the following chapters on Equipment and Materials and Experimental Procedures. The main purpose in this section is to simply identify by type those variables that were treated as a group and generally how they were treated in the experiment. Below are listed the major variables that were consciously attempted to be controlled.

The principle variables are the independent and dependent parameters under observation. They are

1. the vertical transverse distance across the beam (independent) -- x
2. the Int[illegible] (dependent) -- I

The major experimental features are shown in Figure 3. Note in particular the orientation of the coordinate system.

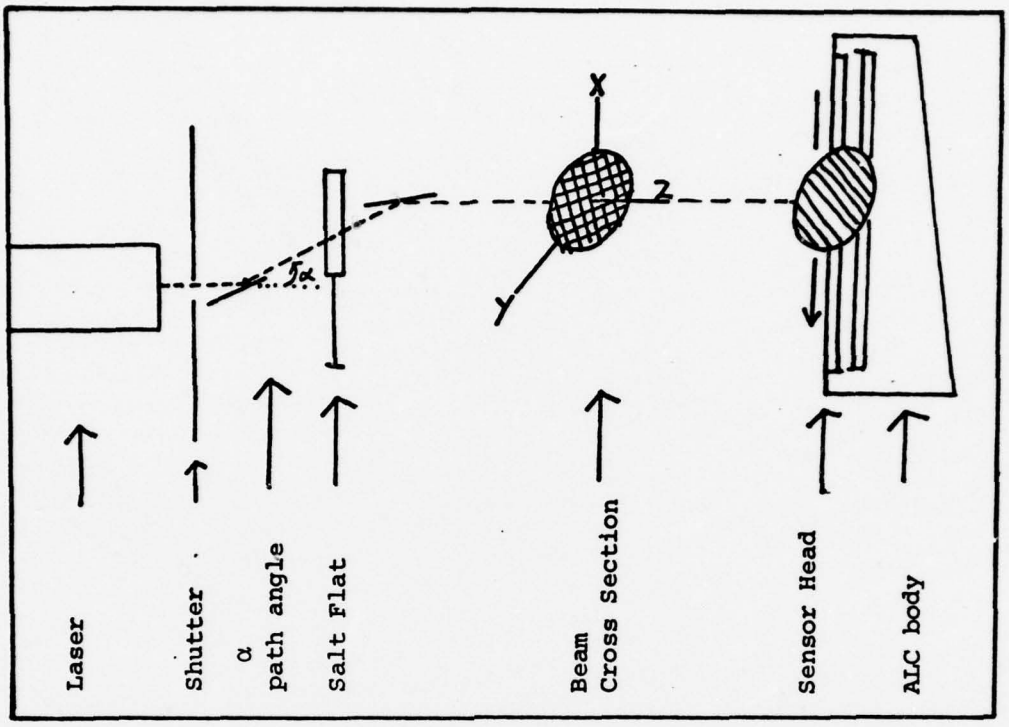

Figure 3. Major Experimental Features

The subsidiary variables are independent variables which are "held constant while an experiment is in progress and given a few discrete values" (Ref. 4:92-93 and Fig. 3). They are

1. the horizontal transverse distance across the beam -- y
2. the distance from the output coupler of the laser to any point on the optical path -- z
3. NaCl beam splitter - henceforth called the Salt Flat -- SF
4. the output power of the laser -- P

The SF has only two discrete values: present or not present. In addition, there were control variables on the laser itself. They were the partial pressures of He, N_2, and CO_2; voltage, gas flow rate, and resonator mirror alignments. These were fixed and never changed for a given output power, and it is assumed that any variation in these variables was accurately reflected in variations in the output power (P) .

The constants are independent variables that were not allowed to change throughout the experiment. See Figure 3 for identification of some of these constants. They were

1. shot duration
2. optical path angle relative to the horizontal α
3. shutter time
4. starting time of the ALC sweep
5. velocity of the sensor head

Assumptions and Approximations

The first assumption is that all other variables not listed in the previous section produce small perturbations and thus are reflected in the experimental error.

The second assumption is that, over the experimental time period, all pertinent temperatures were constant. Temperature control of the laboratory and associated gas lines was held constant at about 70° F. Operating conditions such as repetition rate and cool-down periods were standardized so that an equilibrium temperature was always obtained.

The first approximation is that there is no error associated with x or y. It can be shown (Appendix A) that the relative error (RE) associated with x is .2%, and with y is .79%; therefore, these values were approximated by zero.

The second approximation is that the two flat mirrors and one focusing mirror placed into the optical path at various times do not distort the beam profile. These mirrors are copper based with gold coatings. The deviations from the plane or radial surface are on the order of 150 Å, according to manufacturer's specifications. This is .0014 of the wavelength at 10.6 m. In addition, the absorption coefficient is small (1%) for gold at 10.6 m. Nevertheless, thermal distortion is still minimal since the mirrors are water cooled.

The third approximation is that the statistical error introduced by any of the constant variables listed previously was zero. All times were electronically controlled and any error introduced can be shown to be many orders of magnitude less than the duration of a shot. The other variables were never altered from initial conditions. Other minor assumptions and approximations were made from time to time, and will be so stated as they appear.

Validity

There was anticipated to be a very large number of data points. This large data base permitted the development of a validity concept at three different levels.

Point validity forms the basis for rejection of "bad" profile points. It was found that, after profiles were taken for all admissible

values of the variables seven times each, digitized and $\bar{I}_i$ and σ_i calculated, that there was a total of 13,647 paired values $(\bar{I}_i , \sigma_i)$. This large number gives confidence for rejection of bad data points (Ref. 4:40-41). By averaging all of the σ_i $(\bar{\sigma})$ and calculating the standard deviation of the σ_i (σ^*) , a basis is formed to determine if an individual σ_i is "bad" and, consequently, if $\bar{I}_i$ is bad. This criterion was established as follows:

> If an individual σ_i was greater than $\bar{\sigma} + 3\sigma^*$, then it was classified as an invalid point; therefore, $\bar{I}_i$ was an invalid point.

In a normal Gaussian probability distribution, $3\sigma^*$ represents a 99.7% confidence level for inclusion of valid points. This interpretation gets shaky for small n , but in this instance n is quite large $(= 13,647)$.

Profile validity forms the basis for rejection of a "bad profile." It derives from the definition of a "bad" point. The percentage of bad points in a profile is equal to the number of bad points for a particular profile divided by the number of points in that profile. The criterion was established as follows:

> If an individual beam profile had a percent of invalid points greater than 5%, then it was classified as an invalid profile.

Considering the number of points (13,647) and all potential sources of error (including the digitizing process itself), 5% appeared to be a reasonable (though admittedly arbitrary) figure.

Finally, the experimental validity is defined as the validity of the whole measurement program. Again, its basis lies in the definition of a bad point. A grand percentage can be derived that reflects the total number of bad points divided by the total number of points. This criterion states:

> If the total percentage of bad points was greater than 5%, then in all likelihood, a procedural error had been made and a re-investigation of at least the bad points is indicated.

Again, 5% was chosen as a reasonable figure, based upon the total number of points.

Experimental Constraints

Certain physical constraints were encountered due to the LHMEL permanent structure. All of these constraints confined the optical path to specific pathways within the laboratory space. First, there existed only one experimental position of z for which the optical path was not bent. Thus, for any additional test positions, a flat mirror had to be introduced into the optical path. Second, the present material test position was fixed due to the frequent need of the permanent structured wind tunnel. Objective C requires that this particular position be investigated. This, by necessity, entailed introducing at least three mirrors (normally, two flats and one focusing) into this particular optical path. Last, the laser beam itself enters the test room via a small opening from the laser cell. This necessitates a beam angle of 7.5% through the salt flat.

The salt flat acts as a beam splitter during normal test operations and splits approximately 7% of the total power to a transcient calorimeter. This calorimeter gives real time power readings during a shot. Past material response studies indicate that this salt flat may alter the beam profile to some extent, and thus provisions were made in the experimental design to study what effect, if any, this device had on the beam profile.

IV. Equipment and Materials

The major pieces of equipment used in order of their importance were the Aerotherm Laser Calorimeter, the Ballistic Calorimeter, and the Honeywell 1858 Visicorder. Each will be discussed in turn, giving their basic operating parameters and instrument error. This is followed by a materials section which essentially discusses IR transparency film, Type 577, used in the experiment.

Aerotherm Laser Calorimeter (ALC)

Due to the multi-kilowatt power level of this laser, most operating ranges of the more common detection instruments are exceeded. The ALC was designed for use by the LHMEL and was the prime instrument employed for the profile measurements (see Figure 4). Its main parts consist of a steel frame, traveling sensor head, and an attached rectangular housing containing electronic analogue circuitry.

The basic mechanical action of this apparatus is shown in Figure 5. Across the 5 inch diameter sensor head are seven null point calorimeters (NPC) located colinear and equally spaced. Each NPC is a copper slug measuring 3.18 mm in diameter by 12.70 mm in length with a Chromel-Alumel thermocouple imbedded a short distance beneath the sensing surface. As the sensor head sweeps through the beam, seven output voltages result which are proportional to seven heat flux cross sections, henceforth called channels, of the beam.

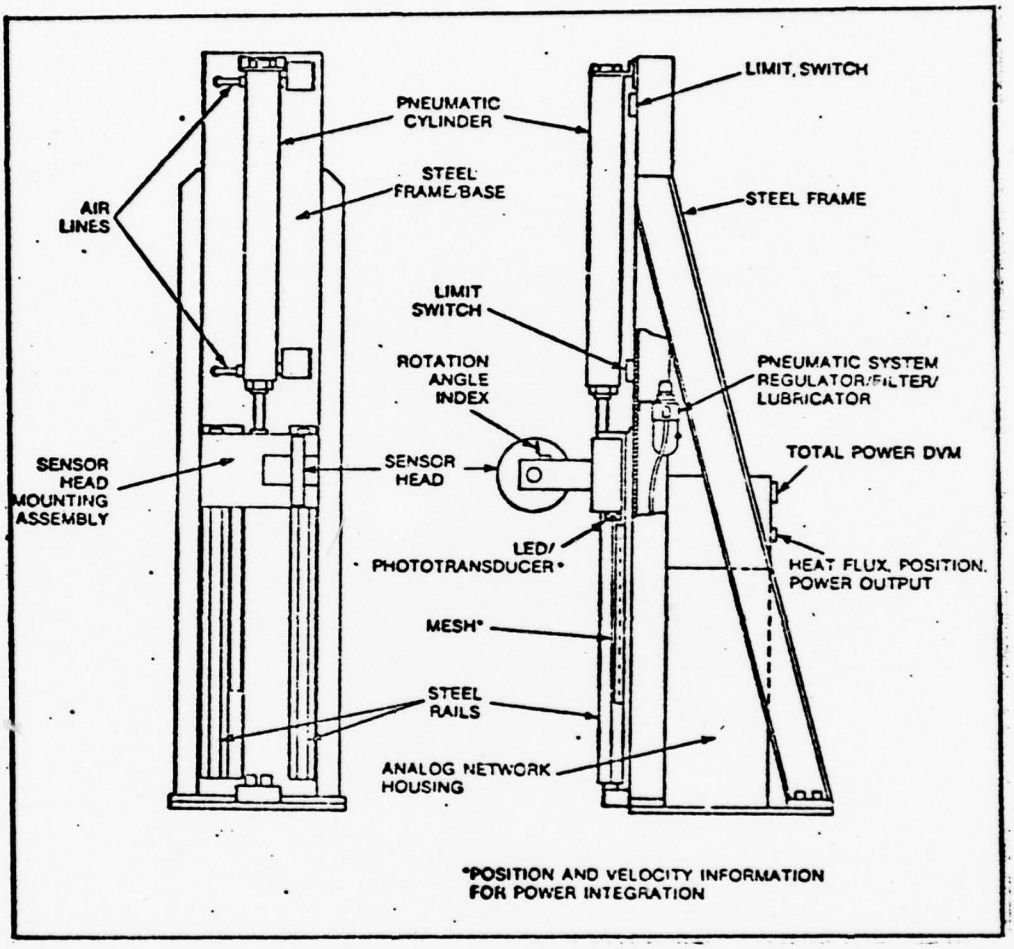

Figure 4. Aerotherm Laser Calorimeter
(Ref 7; Fig. 6)

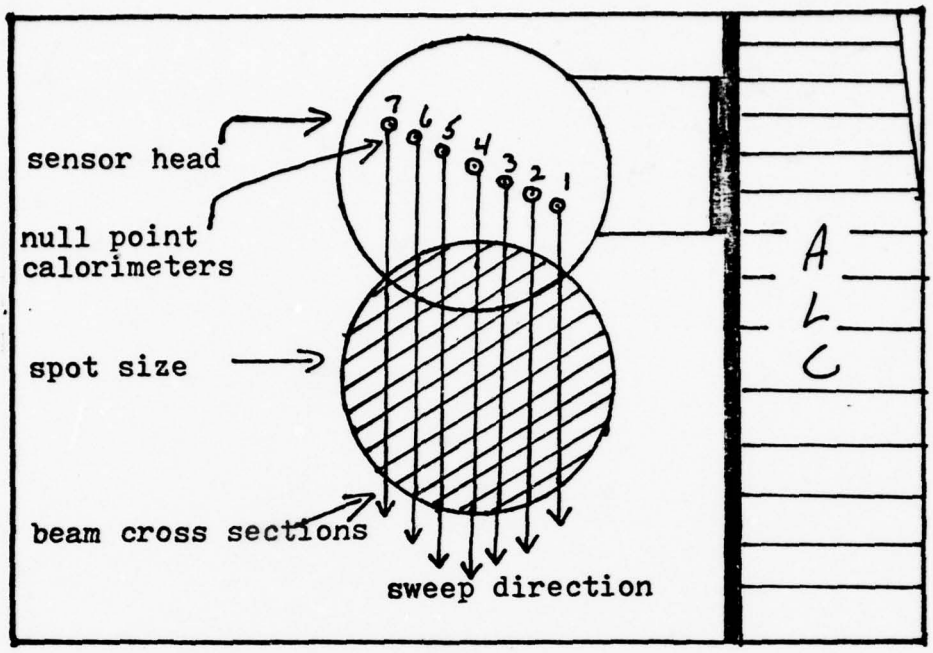

Figure 5. Sensor Head and Beam Cross Sections

A scaling factor of 2.256 converts heat flux (BTU/ft^2-sec) to intensity (w/cm^2). Rotation of the sensor head in the x-y plane is possible which allows for matching the NPCs to the beam spot size. Reference 10 gives a more complete background on the principles of swept null point calorimetry. Due to an integrated circuit malfunction, null point #6 (see Figure 5) was not calibrated. Repair was not possible during the experimental time period. Therefore, data from #6 was discarded.

The ALC is unique in that it uses calibrated analog circuitry to convert each NPC output to heat flux. Conventional NPC data reduction uses digital computer routines. If the ALC is properly calibrated,

instrument error is governed by the electronic response of the analog circuits. This response is 95% in 5 msec. This response time affects the measurements of the leading and trailing edges of the profiles most of all.

Ballistic Calorimeter

The Ballistic Calorimeter was designed to trap radiant beams up to 6.35 cm in radius in order to measure the energy or power (see Figure 6). Its claimed accuracy is 8.74% up to 20 KJ (Ref. 1:42).

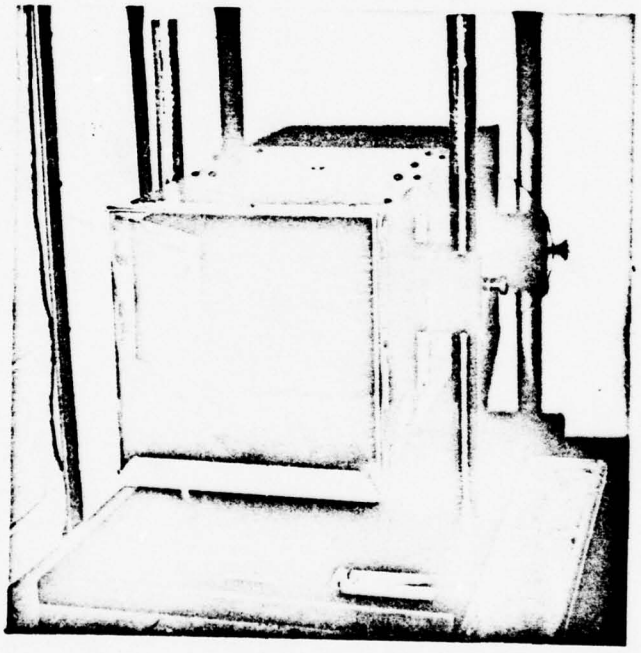

Figure 6. Ballistic Calorimeter

The thermal trap is divided into 24 segments, each with its own thermocouple. This procedure can result in the final answer even before thermal equilibrium is reached. Nevertheless, repeat

time averages 20 minutes for cool down. This instrument was used in the experiment to determine the output power setting at which any given set of shots was made.

Honeywell 1858 Visicorder

The Honeywell Model 1858 is a multichannel recording device that uses a fiber-optic cathode ray tube to trace up to 10 simultaneous data channels on a moving photosensitive paper (Ref. 8:1-1). It makes use of push-in signal conditioning modules which provide a low end sensitivity of 50 mv per major division. The 1858, relative to its own recorded grid lines, has an accuracy of ± .1% on the time scale (abscissa) and ± .5% on the signal scale (ordinate). This instrument recorded the six NPC signals from the ALC. Overall instrument error between the ALC and the 1858, after calibration, was equal to ± 5.64 w/cm^2 .

Materials

One of the simplest ways to obtain intensity profiles for an infrared (IR) laser involves burn patterns on a thermally sensitive material. The distributions are time-averaged as the material oblates; therefore, as quantitative measures, they have low accuracy. Nevertheless, qualitative characteristics of the beam profile are present and are quite instructive. Two such materials are plexiglass and IR transparency film.

The plexiglass material does exhibit to a very low degree of accuracy, some kind of beam profile. Its use in this experiment was strictly as an aid in determining the beam spot size at different

distances along the optical path. This was needed to properly utilize the ALC.

On the other hand, the IR transparency film (3M - Type 577) was very sensitive to variations in the beam profile. Exposure times ran from .01 seconds through .4 seconds with the average about .07 seconds. The characteristics of this film are depicted in Table II, and are included here for any analysis into the material response of this film.

Table II

IR Transparency Film Characteristics

Film Backing	High strength polyester terphthalate
Thickness	.177 mm
Dimensions	216 mm x 267 mm
Color	Light blue tint
Minimum Resolution	3.0 lines/mm
Minimum Image Density	.75 optical density units
Haze	15%

V. Experimental Procedures

This chapter starts out with the general approach whereby the physical layout is delineated by the quantities desired, and the size of statistical base is determined by the measurement precision found acceptable. The next three sections describe precisely how each of the variables listed under Chapter III were measured, their domain or constant values and their associated instrument error. The final section discussed what calculated quantities are needed and how they interrelate.

General Approach

The experiment consisted of measuring the variation of I with x for discrete values of the subsidiary variables y, z, P and SF. The domains of y and z were restricted according to the maximum beam spot size that would not exceed the size of the sensor head. The domain of P never exceeded the maximum of "normal" operating conditions (normal being over 95% of the time). The salt flat was either present or not present.

In addition, the beam profiles obtained during the course of the experiment were divided into two major groups. The first group was obtained from positions along one optical path (positions one through four) while the second group was obtained from positions along a different optical path (positions five through seven) (see Figure 7). The first optical path included only one optical element: a flat mirror. The second optical path was characterized by two flat mirrors

and one focusing mirror. Data obtained via path one was used to determine profile characteristics as a function of distance (z) along the optical path and as a function of power (P) . This path allowed easier positioning of the ALC in addition to possessing only one optical element. Data obtained via path two was used to determine profile characteristics as a function of the salt flat presence and as a function of the normal test position. The present LHMEL facility arrangement dictated the positions of the SF and test plane and, thus, path two was required.

Preliminary analysis into the measurement precision of the experiment gave guidelines to the relative importance of the two sources of error: instrument error and statistical error. It was determined that the instrument error associated with the detection system (see Chapter IV) was $\pm$ 5.64 w/cm^2 . This, by necessity, was the lower limit to the uncertainty of every I vs. x point in any given beam profile. Preliminary profiles were obtained at two different power settings at the same position of z in order to check for statistical fluctuations. The number of shots (n) was chosen as seven for each power setting. The standard deviation (σ) and the standard deviation of the mean (i.e., the standard error - σ_m) were calculated for two positions of x . The results showed that σ ranged from 1.0-4.0 w/cm^2 ; therefore, for the maximum σ (σ(max)) σ_m(max) = $4.0/\sqrt{7}$ = 1.5 w/cm^2 (Ref. 5:71). To reduce σ_m to $\leq$.5 w/cm^2 would require 64 shots for only a 1 w/cm^2 increase in accuracy. Seven shots per selected set of the variables was thus considered an optimum choice, taking into account the available resources and time. The maximum total uncertainty (TU)

of I is given by

$$TU(I) = 5.64 + \sigma(max) = 5.64 + 4. \simeq 10 \text{ w/cm}^2 \quad (6)$$

The maximum intensity for the corresponding I (max) was approximately $\simeq$ 100 w/cm ; therefore, the anticipated relative error of any given point was expected to be about 10%. Moreover, the lower limit to any increases in accuracy was always about 6%.

Principle Variables

The vertical transverse distance x was recorded on the Model 1858 Visicorder. The x measurement origin was arbitrary from power setting to power setting; however, during the data reduction, a common x origin was established for all profiles that were averaged together. This origin was determined by matching leading and trailing edges of the profiles. The domain of x was from 0.0 to 45.7 cm; however, the interval of interest never exceeded 0.0 to 18.0 cm. As stated in Chapter III, the error in x was approximated by zero.

The Intensity I was measured by the ALC for six separate values of y , every time a laser shot was made. This corresponded to six separate cross sections of the beam spot size per shot. All six profiles were recorded on the 1858 Visicorder. The range of I varied from 0.0 to 118.0 w/cm^2 . The number of trials (n) per set of variables was seven. The total uncertainty of I_x (in w/cm^2) is given by

$$TU(I_x) = \pm (5.64 + \sigma_x) \quad (7)$$

where σ_x is the standard deviation of I_x .

Subsidiary Variables

The horizontal transverse distance y assumed six discrete, but arbitrary, values from power setting to power setting. These values identified the particular cross section of the beam spot size which the appropriate null point calorimeter measured. They were arbitrary because they could vary from power setting to power setting; however, the ratio of the particular value to the total beam width never changed. In other words, NPC #2, for example, would always measure the same relative cross section of the beam spot size regardless of its size. Therefore, comparisons could be made between the profiles for any given channel regardless of the values of the other variables. This ratio was maintained by rotating the sensor head a calibrated amount for a given spot size. Insuring the capability to make valid comparisons was the objective; therefore, actual values for y were not measured. Again from Chapter III, the error in y (and thus in the ratio) was assumed to be zero.

The optical path length from the laser output coupler assumed seven discrete values. The ALC positions and associated z values are depicted in Figure 7 and Table III, respectively. The error in z was ± 1.0 cm.

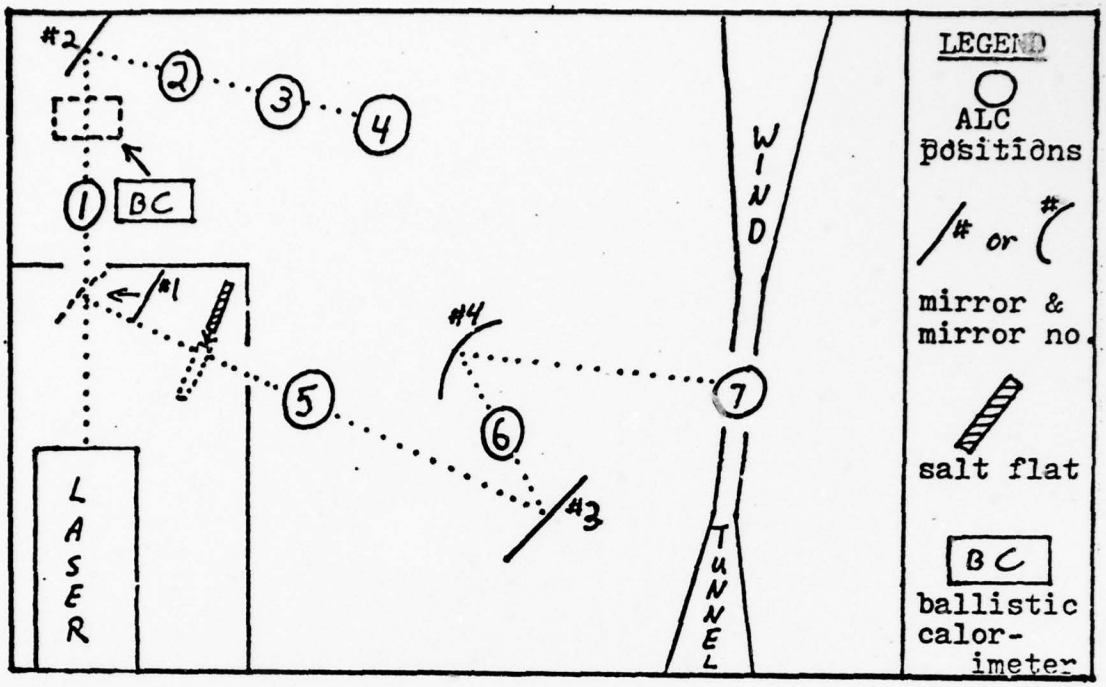

Figure 7. Floor Plan of the LHMEL Depicting ALC Positions in the Experiment

Table III

Values of z

(All measured from the output coupler of the laser along the appropriate optical path -- see Fig. 7)

ALC Positions	z (in meters)
1	2.54 ± .01
2	3.56 ± .01
3	4.57 ± .01
4	5.59 ± .01
5	9.18 ± .01
6	3.56 ± .01
7	5.60 ± .01

The NaCl beam splitter was inserted for only ALC positions 5, 6, and 7. As a control, every position and power setting was repeated without the salt flat presence for these positions.

The output power from the laser was recorded with the ballistic calorimeter. Before and after each series of seven laser shots (or 14 for positions 5, 6, 7), the beam power was measured. As mentioned in Chapter III, the power setting was really a measure of the fluctuations of the control variables. These variables were set at each power setting and held constant through the series of shots. The nominal power settings for which the control variables were set are listed below:

1. for ALC positions one through four, the power settings were 2, 5, 8, 10 and 12 KW.
2. for ALC positions five through seven, the power settings were 5, 8 and 12 KW.

All ballistic calorimeter readings ± 8.74% (the instrument error) were classified by the nominal power setting. If the deviation was greater than 8.74% , then the control variables were readjusted until an acceptable reading was obtained. Due to the excessive turn-around time of the ballistic calorimeter, it was not possible to utilize this instrument between every laser shot; however, data reduction techniques did provide a calculated power value for each shot (see Data Reduction section).

Constants

A list of the variables held constant throughout the experiment and their values is contained in Table IV.

Table IV

Constant Quantities and Their Values

Quantity	Value
Shot Duration	3.0 seconds
Shutter Open Time	1.3 seconds
Starting Time of Sensor Head	Incident with Shutter Opening
Path Angle	7.5° - mirror #1 to mirror #3 0° - all other segments
Velocity of Sensor Head	34.17 cm/sec

Data Reduction

Simple ray matrix analysis yields for the beam divergence the following formula

$$\theta = \tan^{-1} \frac{\Delta x}{R} \qquad (8)$$

where

θ = half-angle beam divergence

R = radius of curvature of the mirror

Δx = diameter of spot size at the focal point of the mirror

(Ref. 11:294-295)

To provide a statistical value for θ , the number of trials was chosen at seven consistent with the reasoning given under the measurement precision paragraph.

Due to the large number of profiles that were obtained, a computer program was developed to reduce the data. The first step was to digitize the beam profiles. Following this, the profiles were reduced to some 266 average profiles and associated standard deviation profiles. (Note: each point on the average curves had its own standard deviation, thus a plot of standard deviations was possible.) Next, a variety of quantities was calculated. A list of these quantiites is given in Table V.

The quantities σ_x , $\bar{\sigma}$, and σ^* were required to meet objective B. Since σ_x represented the deviation of the I_x values about $\bar{I}_x$, σ_x is proportional to the shot stability at point x . Now, the shot stability for all values of x , y , z , SF and P is $\bar{\sigma}$. σ^* indicates the spread of the σ_x values about $\bar{\sigma}$; thus, it is an indicator of how strongly the shot stability is dependent on this group of variables. In addition, the values of $\bar{\sigma}$ and σ^* were used to define the invalid points (see Chapter III). From this, the profile and experimental validities were established. Excluding $\bar{\sigma}$, σ^* , and Δx , the remaining quantities on Table V were used in meeting Objective C. The main idea is to find the "best" plane surface from which the deviations of all associated profiles can be measured. The "best" plane surface is really a "better" plane surface since only a sampling of points (five) was selected to characterize a profile. A weighted approach to all these calculations was

Table V

List of Calculated Quantities

(Consult Appendix A for the Actual Equations)

Symbol	Meaning	Objective needed for
$\bar{I}_x$	Average value of I at x	A,B,C,D
σ_x	Standard deviation of I at x	B,C
$\bar{\sigma}$	Average value of all σ_x's gathered	B
σ^*	Standard deviation of σ_x's	B
m_i	Slope from weighted least squares fit	C
b_i	Intercept from weighted least squares fit	C
$\bar{m}$	Weighted average of m_i for six channels per power setting	C
$\bar{b}$	Weighted average of b_i for six channels per power setting	C
b_{io}	Intercept from weighted least squares fit assuming m = 0	C
$\bar{b}_o$	Weighted average of b_{io} for six channels per power setting	C
σ_{mb}	Weighted standard deviation about the line described by $\bar{m}$ and $\bar{b}$	C
σ_o	Weighted standard deviation about the line described by m = 0 and $\bar{b}_o$	C
$RE(\sigma_{mb})$	Relative error of σ_{mb} over midpoint value of line described by m and b	C
$RE(\sigma_o)$	Relative Error of σ_o over value of b_o	C
Δx	Diameter of beam at R/2 of a selected mirror	A

necessary since each $\bar{I}_x$ had an associated σ_x which were not all the same (consult Appendix A for the exact equations). The end results are the quantities $RE(\sigma_{mb})$ and $RE(\sigma_o)$ which are the relative errors measured against two kinds of "best" plane surfaces. The first kind is a "tilted" flat top surface, while the second is a true flat top surface.

Finally, the output power was calculated in accordance with Equation (23), Appendix B, for each laser shot.

VI. Results

This chapter gives the experimental results from the two detection instruments: the transparency materials and the Aerotherm Laser Calorimeter. This is followed by a discussion of results in which the essential features are summarized and certain observations are made. The results conclude with an error analysis.

Transparency Material Results

The results obtained using the IR transparency film were used exclusively to derive both the beam divergence and the qualitative characteristics of the two-dimensional (2-D) beam profiles. The beam divergence was obtained in accordance with Equation (8). The results are shown below

Table VI

Beam Divergence Results

Number of Shots = n = 7
Average Beam Divergence = $\bar{\theta}$ = 3.75 mrad
Standard Deviation = σ_θ = ± .03 mrad

In determining the qualitative characteristics in a particular 2-D beam profile, the following characteristics were observed in the transparencies (see Figure 8). They were

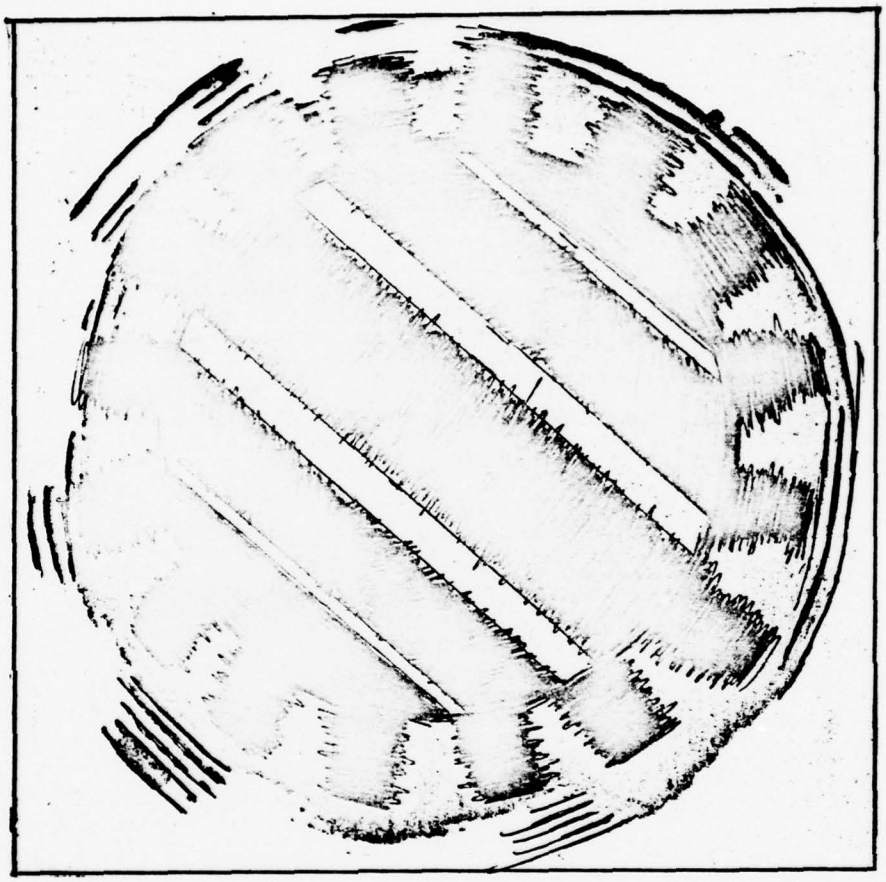

Figure 8. Schematic - Observed Beam Characteristics

Power - 10 KW ALC Position - #4

(Note: This schematic has been artistically enhanced to show the major components. The circular ring pattern can be partially observed around the outer edges; the angular and rectangular patterns are shown in entirety.)

1. A radially symmetrical ring pattern existed with the number of rings on the order of 50.
2. An angular radial pattern existed in most transparencies with the number of lobes on the order of 16.
3. Four distinct minimums were observed in most transparencies on an axis at +45° to the horizontal. No minimums were observed on axes at -45° to the horizontal.

Characteristic three will be referred to as the rectangular component, and the characteristics one and two as the radial component. Upon comparing transparencies for the beam characteristics as a function of z and as a function of P , the following was found.

1. As a function of z , the rectangular component decreased as z increased. No change was observed in the radial component.
2. As a function of P , the rectangular component increased as P increased. No change was observed in the radial component.

Upon comparing transparencies for the beam characteristics as a function of P and SF , these results were found:

1. The same basic beam characteristics as noted earlier.
2. No observable change from one profile to another, either as a function of P and/or SF .

In the process of a laser exposure, the IR transparency film invariably is thermally stressed and thus is not suitable for inclusion in a written report. To date, a suitable presentation form has not been found; however, the appropriate transparency exposures are on file at the LHMEL laboratory and are available for inspection.

ALC Results

The more precise quantitative results from the Aerotherm Laser Calorimeter were used to get the results for Objectives B, C, and D. Each, in turn, will be discussed in this section.

For Objective B, the indicator of shot stability for all values of the independent variables is $\bar{\sigma}$. σ^* , the standard deviation of the standard deviations, is indicative of how strongly the shot stability is dependent upon these variables. The integer value of n represented the total number of σ_x values averaged to $\bar{\sigma}$. The results are shown below.

Table VII

Shot Stability Results

$\bar{\sigma}$	=	$\pm$ 6.90 w/cm^2
σ^*	=	$\pm$ .83 w/cm^2
n	=	13,674

For Objective C, a number of additional comments are required in order to obtain the proper perspective regarding these results. First, the data reduction procedures "sampled" five points along any given profile. Thus, any values derived are truly an estimate only of the variation found. Second, the normal test position is position number five in Figure 7. Third, normal operating LHMEL procedures made use of the salt flat; therefore, only those profiles were tested for variations. Fourth, the mode of testing was a weighted least square fit (see Appendix A) of two types. Method one allowed both m and b to be established by the methodology. This was to check if the "best" flat top fit was actually slanted. The second method assumed $m = 0$ and only allowed b to be established by the methodology. This insured a perfectly uniform standard from which the variations could be measured. The results of both methods are presented for comparison. Fifth, a weighted standard deviation (see Appendix A) about the lines $y = \bar{m}x + \bar{b}$ and $y = \bar{b}_o$ were taken as a measure of the degree of variation. Finally, the values $\overline{RE}_{mb}$ and $\overline{RE}_{b}$ represent the average relative errors of the variation for all channels at a given power setting. The results are depicted in Table VIII.

For objective D, the total number of average profiles calculated was 228. If the only objects of this effort were A, B , and C , then three positions at about four power settings would have been adequate for a total of about 84 APs. The reasons for establishing a large data base were given in the Introduction. In addition, the large number of data points lends a large confidence in the tests for validity. The complete set of average profiles will be on file at the

Table VIII

Measured Variation Results

(At ALC Position #5)

Power	Method One			Method Two		
	$\bar{m}$(w/cm^2)	$\bar{b}$(w/cm^2)	$\overline{RE}_{mb}$(%)	$\bar{m}$(w/cm^2)	$\bar{b}_o$(w/cm^2)	$\overline{RE}_b$(%)
12 KW	3.09	68.84	11.9	0	90.37	11.2
8 KW	1.93	45.88	13.6	0	57.16	12.0
5 KW	1.87	22.85	15.1	0	33.14	14.9

LHMEL and will be available to bona fide users upon demand. A subset of 96 APs have been chosen for inclusion in this work. The complete subset can be found in Appendix B. In addition to the above, the results of the validity tests defined in Chapter III were calculated and are listed in Table IX.

Table IX

Validity Test Results

	Total Number Of	Number Invalid	Percent
Points	13,647	214	1.57
Profiles	228	20	8.77

Of the twenty bad profiles, eight were found in channel 7, eight in channel 2, and one each in channels 1, 3, 4, 5.

Finally, power calculations were made from the APs for each laser shot. The total number of laser shots made was 266; therefore, a listing of each calculated power value will not be made. The results can be summarized, however, by stating that all calculations were within ± 8.74% of the ballistic calorimeter readings. Thus, the calculated values of the power fell within the instrument error of the experimental values.

Discussion

Due to the predominant radial and angular components present in the beam pattern, the more appropriate form of Equation (2) would be the Gaussion-Laguerre form in circular polar coordinates (Ref. 12:29). The parameters p and ℓ in this equation correspond to m and n from the rectangular form and represent the number of nodes present in the spatial pattern in the raidal and angular directions, respectively. The number of rings present was on the order of 50. The number of angular intensity lobes was on the order of 16. This suggests that the values of p and ℓ are on the order of 50 and 16, respectively.

Another alternative can explain the 16 observed angular lobes, i.e., there are also 16 anodes equally spaced about each end of the resonator. If the angular positions of the observed lobes corresponded exactly with the anode positions, then the observed lobe pattern is produced by a node volume shaped by the positions of the anodes. Various laser transparency shots were taken with appropriate anodes disconnected to test this hypothesis.

The results were mixed. Partial correspondence existed between the anode and lobe positions for about 10-12 lobes. The remaining positions did not correspond at all. In addition, some lobe pattern was observed even for lobe positions which corresponded to disconnected anode positions. Apparently, a combination of pure angular modes with an anode-shape mode volume accounts for the observed angular lobe pattern.

In addition to the circular modes present, the beam displayed a rectangular component suggestive of a lower order rectangular mode. Since any Laguerre modes can be represented as a linear combination of a certain number of rectangular modes (Ref. 2:331), such an effect is not unexpected. For reasons unknown, however, certain rectangular modes of the form $m = 4$ and $n = 0$ are more energetic in comparison to all the other rectangular modes present. As the power is increased, presumably all modes become more energetic equally and the dominance effect of any one is reduced. Yet, the opposite effect was observed. Therefore, there is apparently some energetic selection mechanism in effect favoring the rectangular mode or modes observed. As a function of distance, the rectangular effect should become less dominant as compared to the sum of all other modes. This is what was observed. As a function of the salt flat, a careful analysis into the actual number of modes present and the Laguerre form of Equation (2) would need to be done to explain the null effect observed.

In addition, the ALC results do support (although to a lesser degree) the beam characteristics observed in the IR transparency film. Since the sweep direction of any given null point would cross the rectangular intensity pattern at about 45°, the average profiles of

channels one through seven should display one or, at most, two maximums per channel. Generally, this quality is reflected in the average profiles (AP). Refer to Appendix B and select any profile from channels three, four and five. Channels one and seven fell at the edges of the beam and, therefore, did not cross the area of interest. Channel six data does not exist (see Chapter IV).

In summary, the beam divergence was found to be 3.75 milliradians. The overall beam characteristics appear to have radial and angular components with a low order rectangular component superimposed. Whatever effect distance and power had, they appeared to affect this rectangular component the most. Furthermore, the effect of each was opposite. P increases the dominance of this factor while Z decreases it. The shot stability was found to be about $\pm$ 7. w/cm^2 with about a 1. w/cm^2 deviation. The estimate on the extent of variation showed that the relative errors varied from about 11% to 15%, regardless of the method used. The percentages do show a slight reduction trend as the power setting increases.

Error Analysis

The uncertainty in any given $\bar{I}_x$, ranged from the minimum limit of $\pm$ 5.64 w/cm^2 through as high as 18. or 19. w/cm^2 at a few points. The vast majority of σ_xs clustered near the minimum range or, as indicated in Objective B, $\bar{\sigma} = \pm 6.90 \pm .83$ w/cm^2. The data does indicate that consistently larger values of σ_x were observed at the leading and trailing edges of the average profiles; that is, the standard deviations plots for any given AP "peaked" at the start and end of a profile.

The validity results from Table VII indicate the percentage of invalid points was 1.57% . This is less than the 5% criterion established in Chapter III as being a reasonable value for the validity of the experiment. Thus, it is reasonably certain that no procedural errors were made. The percentage of invalid profiles was higher at 8.77% . In particular, two channels had the bulk of the "bad" profiles. It appears that what error did exist happended in sporadic bursts to two specific channels (two and seven). Possible explanation might be that extraneous lab signals affected these two channels from time to time. An electrical check of the ALC or 1858 Visicorder is indicated.

The largest source of error was the instrument error. The stastical error yielded results of about 1.3 w/cm^2 on the average. Any future effort should be directed at reducing the instrument error to this magnitude before any increase in the number of trials is done.

There was one source of systematic error apparent: the absorptivity coefficient of the sensor head changed at unknown points in the experiment. The sensor head is covered with "Black Magic" copper oxide coating that deteriorated over the course of the experiment (see Figure 9). The absorptivity coefficient was known prior to the experiment and it was measured after the experiment; however, the exact values were not known from shot to shot.

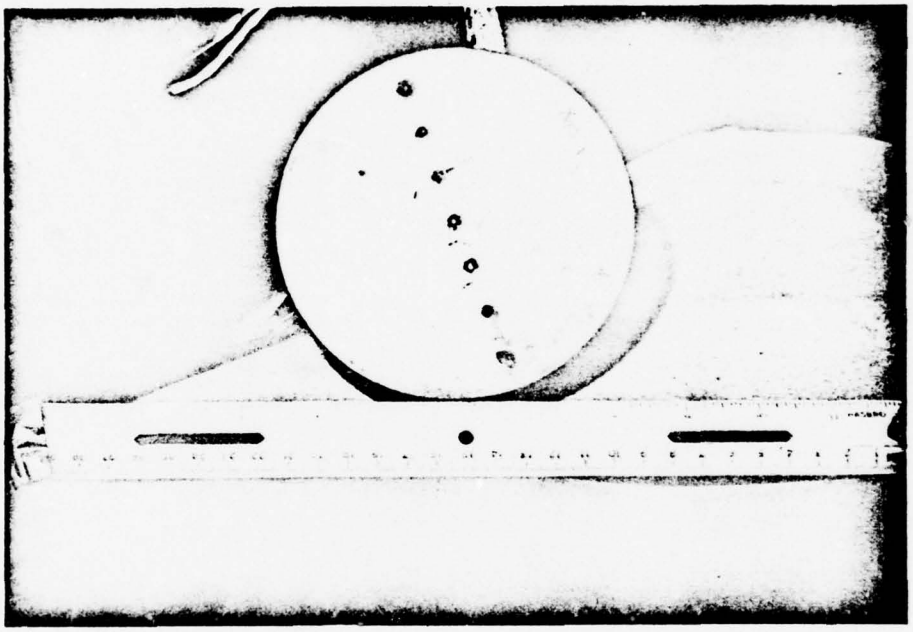

Figure 9. Sensor Head Coating Deterioration

VII. Conclusions and Recommendations

The half-angle beam divergence was calculated to be 3.75 mrad with a ± .03 mrad standard deviation. The present value used by the LHMEL personnel has been 4.0 mrad ± .5 mrad . Considering that the 3.75 value is statistically derived and in agreement with a previous value suggests that this figure is highly reliable.

The beam profile is describable in terms of three experimentally distinguishable characteristics labeled the circular, angular and rectangular components. The circular and angular patterns do not appear to be functions of the output power, the optical path distance or presence of the salt flat. The rectangular component does bear some functional relationship to the power and optical path distance. It is proportional to P and inversely proportional to z.

The shot stability was calculated to be ± 6.90 w/cm^2 . However, the major part of this error (± 5.64) was the instrument error. Thus, the statistical fluctuation was on the order of 1.3 w/cm^2 . Considering this is a multikilowatt laser, this value indicates that the LHMEL laser is exceptionally stable. Moreover, the value ± .83 w/cm^2 for σ^* indicates that the shot stability is relatively constant over the operating ranges of the variables tested.

The estimate of the variations from an idealized flat top profile indicated a relative error on the magnitude of 11% to 15% . A statement made by D. C. Rabe in his report on the performance of this laser (Ref. 12:1) indicated a variation of only 5% . An exact comparison cannot be made between the two figures since his methodology

is not stated. A possible cause for this apparent discrepancy could be in the "estimate" procedure used in this effort. If the total number of data points on a given cross-section were used (around 60), the end result could lower the range of the variation.

An extended data base has been shown to exist with a high reliability. Over 228 average profiles were experimentally derived covering the normal LHMEL operating ranges of the variables investigated. Furthermore, only 1.57% of all the data points were found invalid, indicating that this data base is highly reliable. Future efforts can begin with immediate data available, and thus avoid any delays.

Finally, the main objective was to investigate the extent of the profile variations, thereby determining if the variations were large enough to be significant in material response. The acceptability or non-acceptability of the 11 to 15% relative errors can only be determined for the user by his own experimental criteria. However, the ultimate objective of the LHMEL laboratory is to produce the best flat top profile possible. Past indicators suggest that a lower value of the variations existed. Therefore, of the three possible courses of action mentioned in the Introduction, the conclusion reached is that the second alternative applied; that is, the variation found indicates that a more precise analysis of the data is advisable.

The first recommendation is that any effort attempted to increase the uniformity of the beam be aimed at reducing the rectangular component found in the beam profile. The easiest way of going about this would be to adjust the cavity mirrors to perfect alignment about the cavity axis. This condition is required for pure circular modes. Second, improvements in experimental design can be made by reducing the instrument error.

With the present equipment, the total instrument error is restricted by the response time of the null point calorimeters in the ALC (about 1-2 msec). The circular ring pattern at recommended sweep speeds is transversed at the rate of .5 - 1. msec per ring. A more responsive detection instrument will be necessary to study the circular component of the beam profile. Third, the systematic error should be reduced by determining some rate of deterioration as a function of number of shots, or by determining some practical method of determining the absorptivity coefficient from shot to shot. Fourth, increased efficiency can be realized by providing for digitized output on tape as the immediate product.

Finally, as stated in the conclusions, further analysis is recommended. A computer program should be devised to calculate the relative error for all positions and power settings. The results could be used to identify the combination of power and distance for the best "flat top" profile.

Bibliography

1. Air Force Materials Laboratory. The Laser Hardened Materials Evaluation Laboratory - Information for Users. AFML/LPJ TM-78-2. Wright-Patterson Air Force Base, Ohio:Laser Hardened Materials Branch, November 1977.

2. Air Force Systems Command. Experimental Performance of a 15 Kilowatt CW CO_2 Electric Discharge Laser. Wright-Patterson Air Force Base, Ohio: Air Force Aero Propulsion Laboratory, November 1977.

3. Air Force Systems Command. A 15 Kilowatt CW CO_2 Coaxial Electric Discharge Laser. AFWL-TR-76-115. Kirtland Air Force Base, NM: Air Force Weapons Laboratory, August 1976.

4. Baird, D.C. Experimentation: An Introduction to Measurement Theory and Experiment Design. Englewood Cliffs: Prentice Hall, Inc., 1962.

5. Bevington, Philip R. Data Reduction and Error Analysis for the Physical Sciences. New York: McGraw-Hill Book Company, 1969.

6. Foster, T. Operation Manual Aerotherm Laser Calorimeter. UM-76-79. Wright-Patterson Air Force Base, 1976.

7. Foster, Thomas F., John E. Arnold and Edmund J. Rolinski. "A New Approach to Laser Beam Heat Flux and Power Profiling," Paper presented at ISA International Instrumentation Symposium, Albuquerque, NM, 1-4 May 1978.

8. Honeywell, Technical Manual, Model 1858, Graphic Data Acquisition System, Maintenance Instructions. Denver: March 1975.

9. Kogelnik, H., Li Tingye. "Laser Beams and Resonators," Proc. IEEE, Appl. Opt., 54: 1312-1329 (October 1966).

10. Powars, Charles A., William S. Kennedy and Roald A. Rindal. "Heat Flux Measurement Using Swept Null Point Calorimetry," Journal of Spacecraft and Rockets, 9 (9): 668-672 (September 1972).

11. Siegman, A.E. An Introduction to Lasers and Masers. New York: McGraw-Hill Book Company, 1971.

12. Weichel, H., and L.S. Pedrotti, "A Summary of Useful Laser Equations - An LIA Report," Electro-Optical Systems Design: 23-35 (July 1976).

13. Wilson, E. Bright, Jr. An Introduction to Scientific Research. New York: McGraw-Hill Book Company, 1952.

Appendix A

Miscellaneous Parameters

Error Analysis of x and y

The 1858 Visicorder has a ± .1% error relative to its own abscissa scale. The scaling factor was .1 second/division yielding a .001 second error. The sweep velocity was 34.17 cm/sec ; therefore, the error in $x = (.001)(34.17) = .0347$ cm . The scale ranged up to 13.67 cm , giving a relative error of ± .2% .

The error in y was estimated as ± .1 cm . The width of the sensor head is 12.7 cm , giving a relative error = .79% .

Equations of Interest

The following is a list of pertinent equations including the equation for calculating the power (see pp.

$$\sigma_x = \left[\frac{\sum (y_x - \bar{y})^2}{n - 1} \right]^{\frac{1}{2}} \tag{9}$$

where

$\bar{y}$ = average of y_x values

n = number of trials

y_x = individual values at x

$$\bar{\sigma} = \frac{\sum_{i}^{n} \sigma_x}{n} \tag{10}$$

$$\sigma^* = \left[\frac{\sum (\sigma_x - \bar{\sigma})^2}{n - 1} \right]^{\frac{1}{2}} \tag{11}$$

$$m = \frac{(\sum x_i y_i/\sigma_i^2)(\sum 1/\sigma_i^2) - (\sum y_i/\sigma_i^2)(\sum x_i/\sigma_i^2)}{(\sum 1/\sigma_i^2)(\sum x_i^2/\sigma_i^2) - (\sum x_i/\sigma_i^2)} \tag{12}$$

where

x_i, y_i = coordinate pair

$$b = \frac{(\sum x_i^2/\sigma_i^2)(\sum y_i/\sigma_i^2) - (\sum x_i/\sigma_i^2)(\sum x_i y_i/\sigma_i^2)}{(\sum 1/\sigma_i^2)(\sum x_i^2/\sigma_i^2) - (\sum x_i/\sigma_i^2)^2} \tag{13}$$

$$\bar{m} = \sum w_i m_i \qquad \text{(Ref 13:219)} \tag{14}$$

where

m_i = individual slopes

w_i = weighting coefficient (15)

$$\bar{b} = \sum w_i b_i \tag{16}$$

$$b_{io} = \frac{\sum y_i/\sigma_i^2}{\sum 1/\sigma_i^2} \tag{17}$$

$$\bar{b}_o = \sum w_i b_{io} \tag{18}$$

$$\sigma_{mb} = \left[\frac{\sum 1/\sigma_i^2 \, (y_i - \bar{m}x_i - \bar{b})^2}{(n-2) \sum 1/\sigma_i^2} \right]^{\frac{1}{2}} \tag{19}$$

$$\sigma_o = \left[\frac{\sum (y_i - \bar{b}_o)^2/\sigma_i^2}{(n-2) \sum 1/\sigma_i^2} \right]^{\frac{1}{2}} \tag{20}$$

$$RE(\sigma_{mb}) = \sigma_{mb}/y_j \tag{21}$$

where

y_j = midpoint value of line described by m and b

$$RE(\sigma_o) = \sigma_o/y_k \tag{22}$$

where

y_k = midpoint value of line described by $m = 0$ and b_o

$$P = d \sin \phi \int_0^\infty \sum_{i=1}^{7} \dot{q}_i \, \frac{dx}{dt} \, dt \tag{23}$$

where

d = separation between null point calorimeters (NPC)

$\sin \phi$ = angle between vertical and line of NPCs

$\dot{q}$ = heat flux

dx/dt = sweep velocity = 34.17 cm/sec

P = power

Appendix B

ALC Profile Results

The object of this appendix is to present a basic subset of the beam profiles obtained in fulfillment of objective D. The complete set of beam profiles is on file at the Laser Hardened Materials Laboratory and is available to bona fide users. The profiles included here are divided into two groups.

The first group consists of four profiles per page, representing ALC positions one through four. There is one channel per page with only channels three, four and five being represented. There are three pages per power setting covering 2, 5, 8, 10, and 12 kilowatts. The NaCl beam splitter was not present in the optical path for this group.

The second group consists of three profiles per page representing ALC positions five through seven. Again, there is only one channel per page of channels three, four, and five. There are three pages per power setting covering 5, 8, and 12 kilowatts. The NaCl beam splitter was present in the optical path for this group.

The profile sets are identified by a profile set number in the following manner:

1. The first digit will always be a one or two, which means
   a. One -- belongs to Group One
   b. Two -- belongs to Group Two
2. Following the dash, the power setting is given (in KW)
3. Following the second dash, the channel number is given (No. 1 through 7).

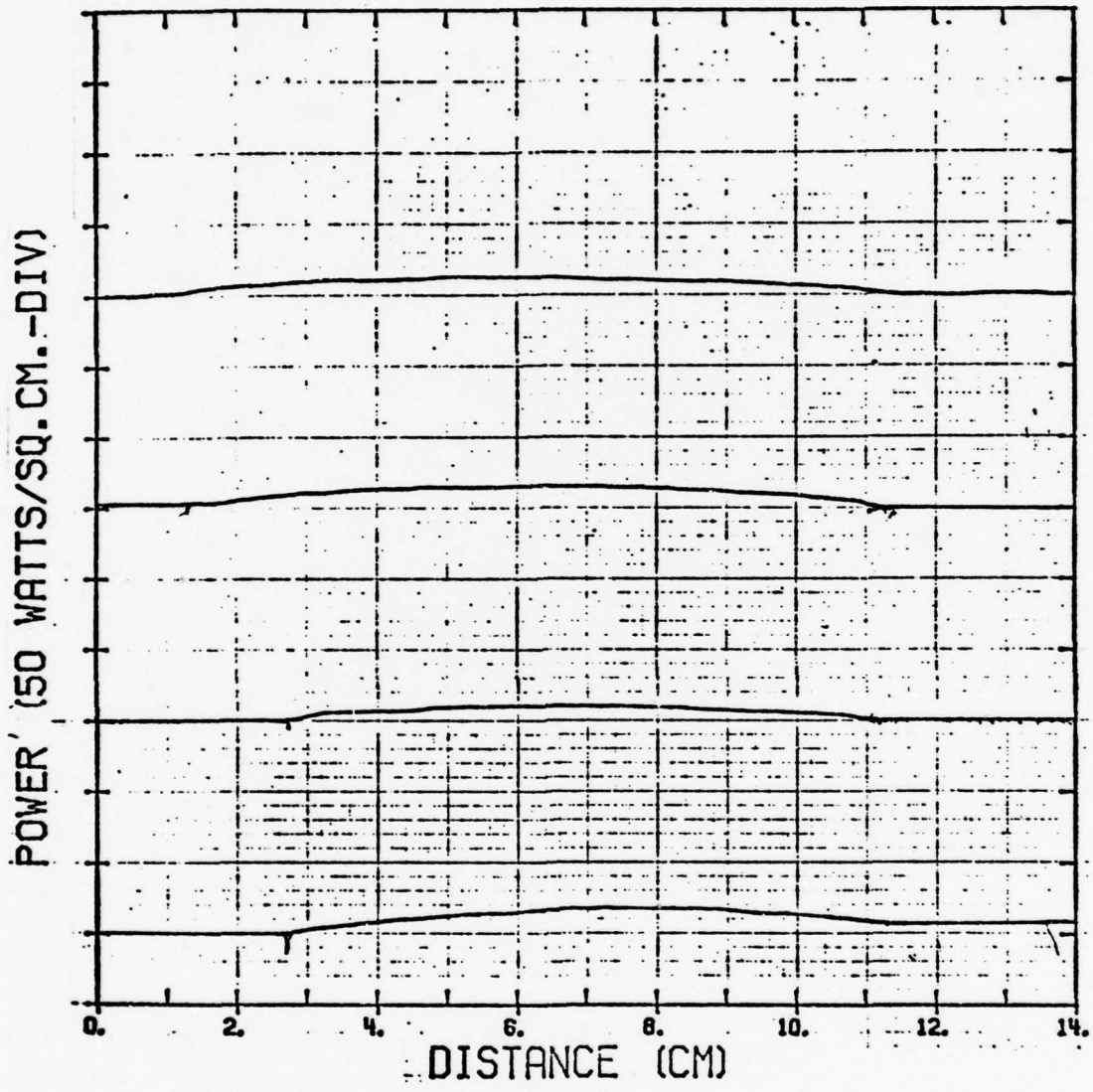

Figure B-1. Profile Set 1-2-3

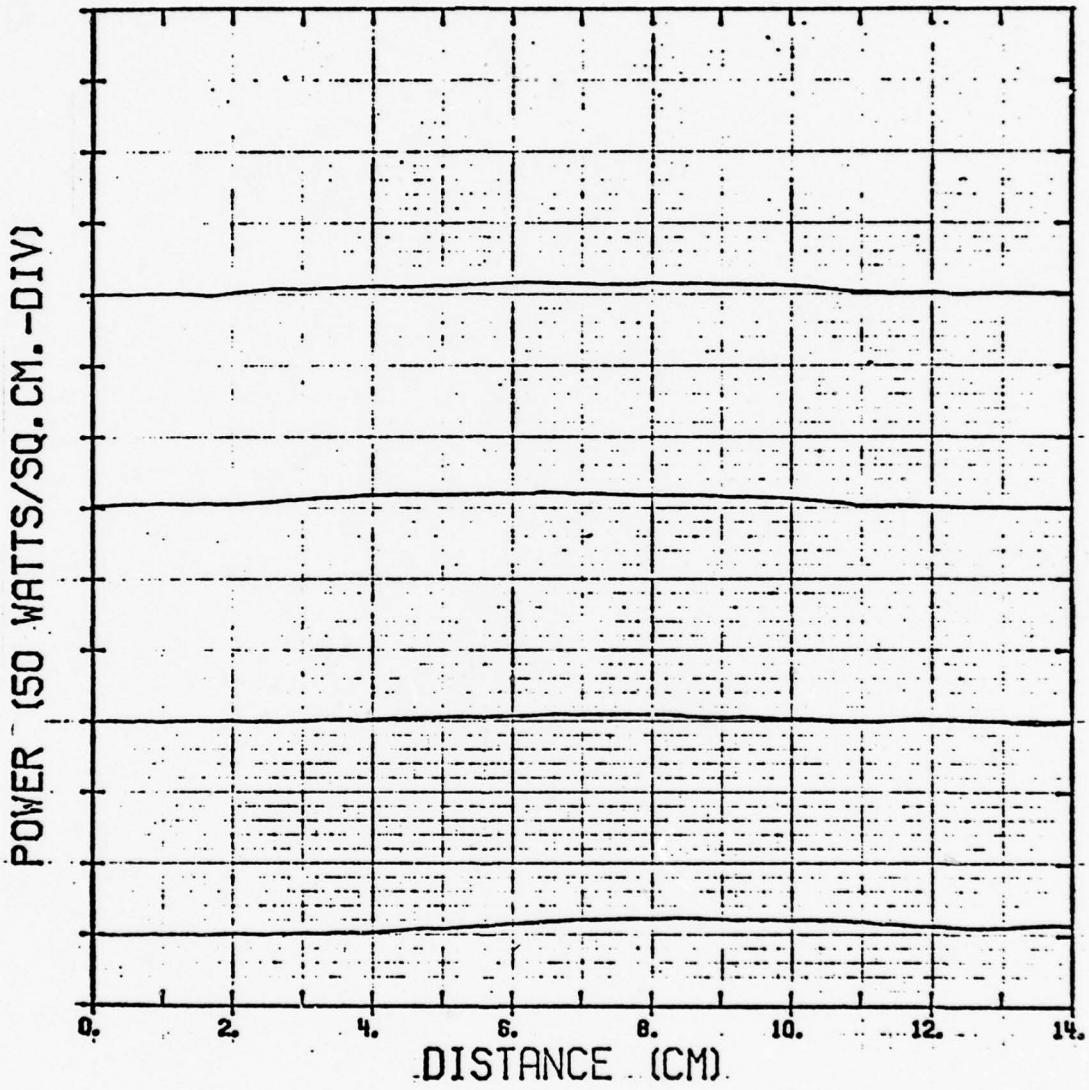

Figure B-2. Profile Set 1-2-4

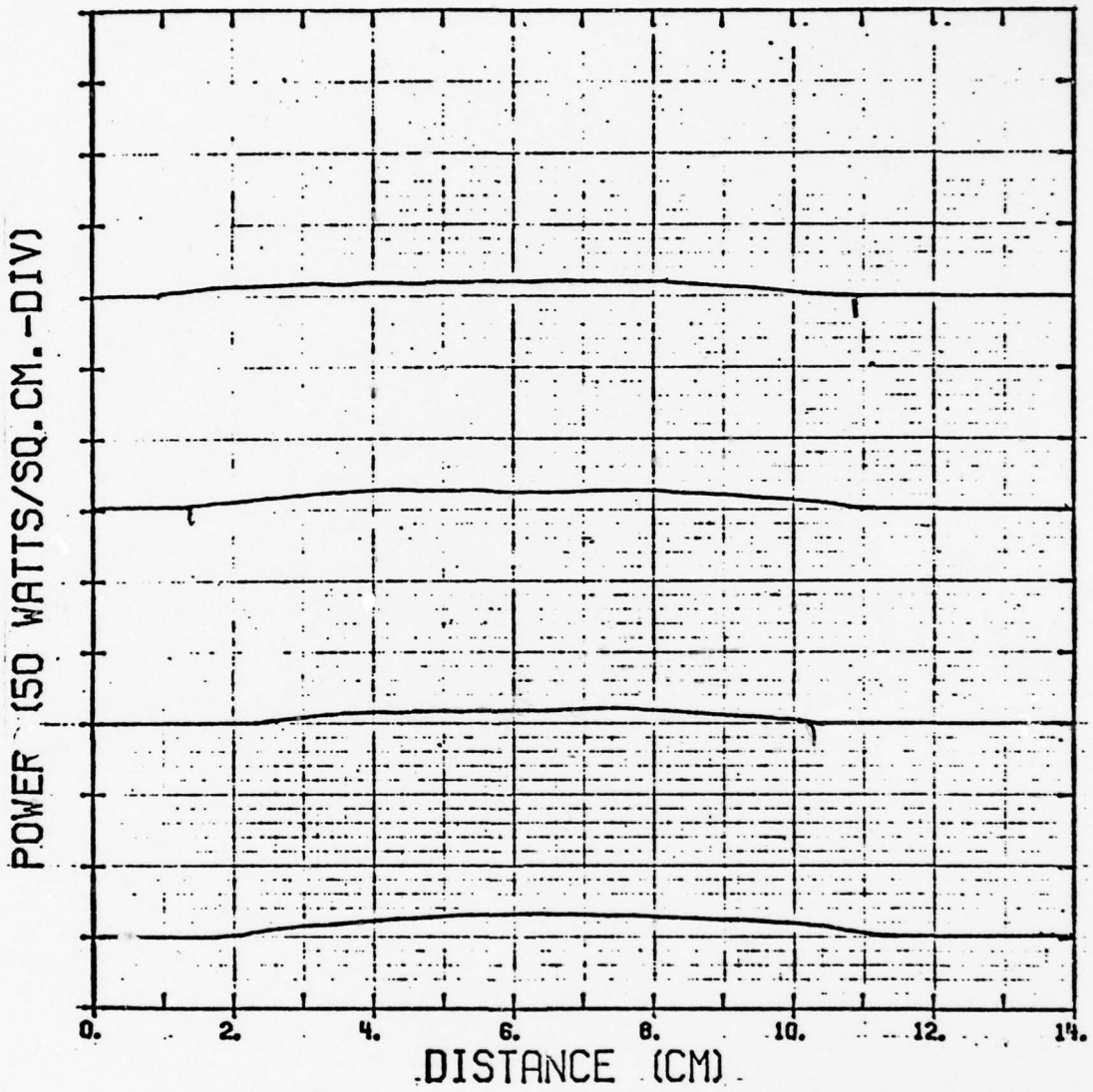

Figure B-3. Profile Set 1-2-5

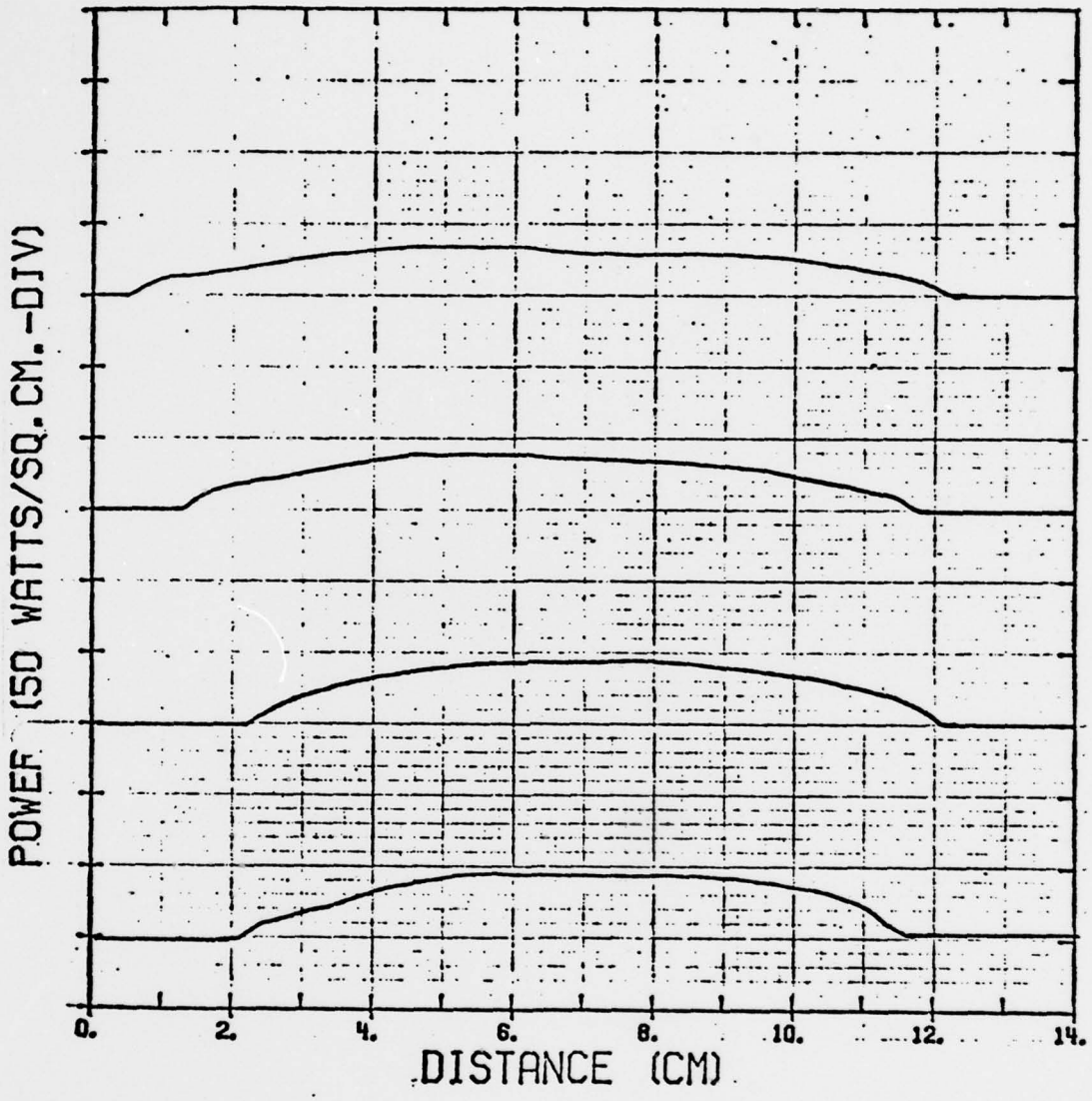

Figure B-4. Profile Set 1-5-3

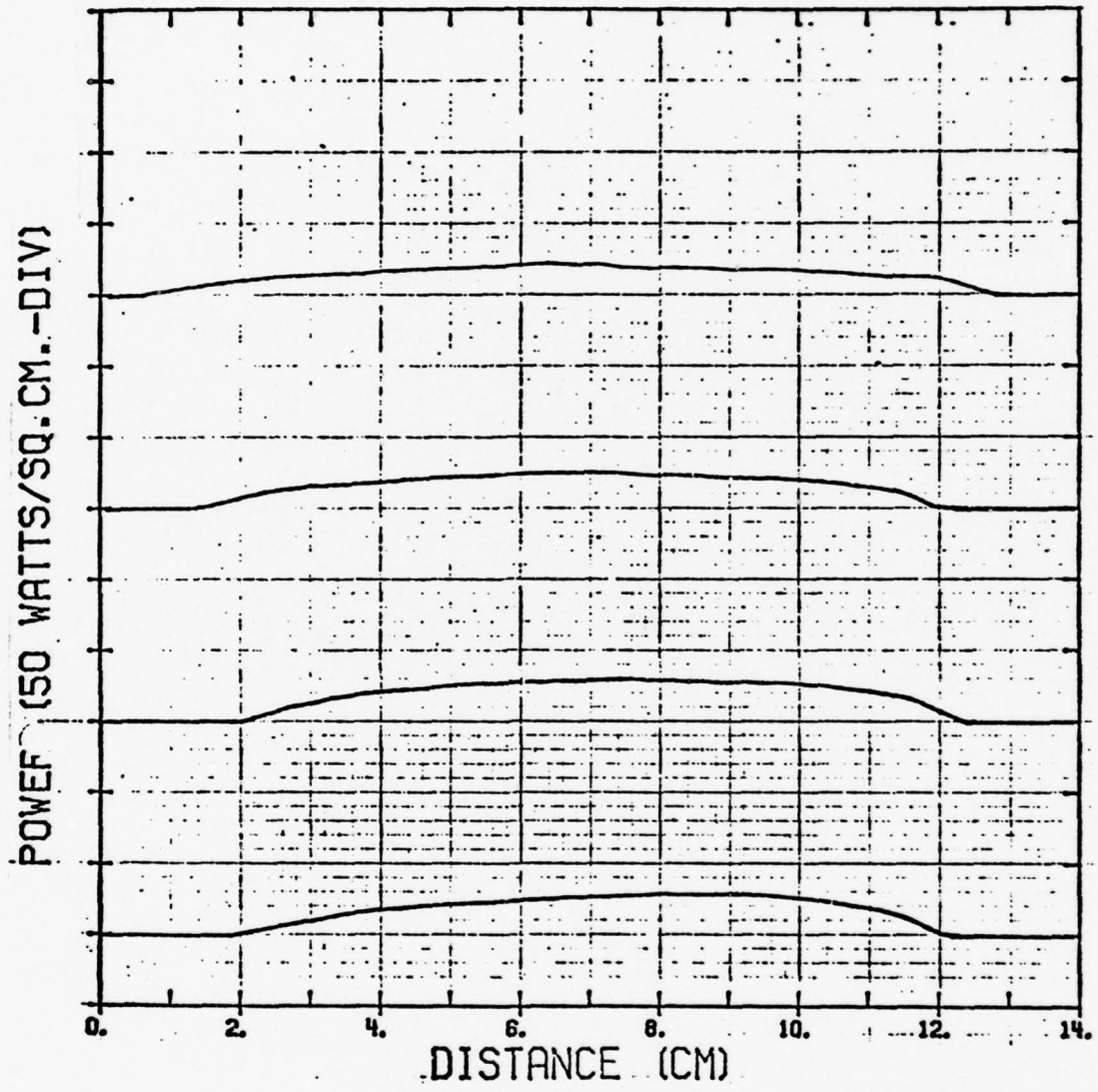

Figure B-5. Profile Set 1-5-4

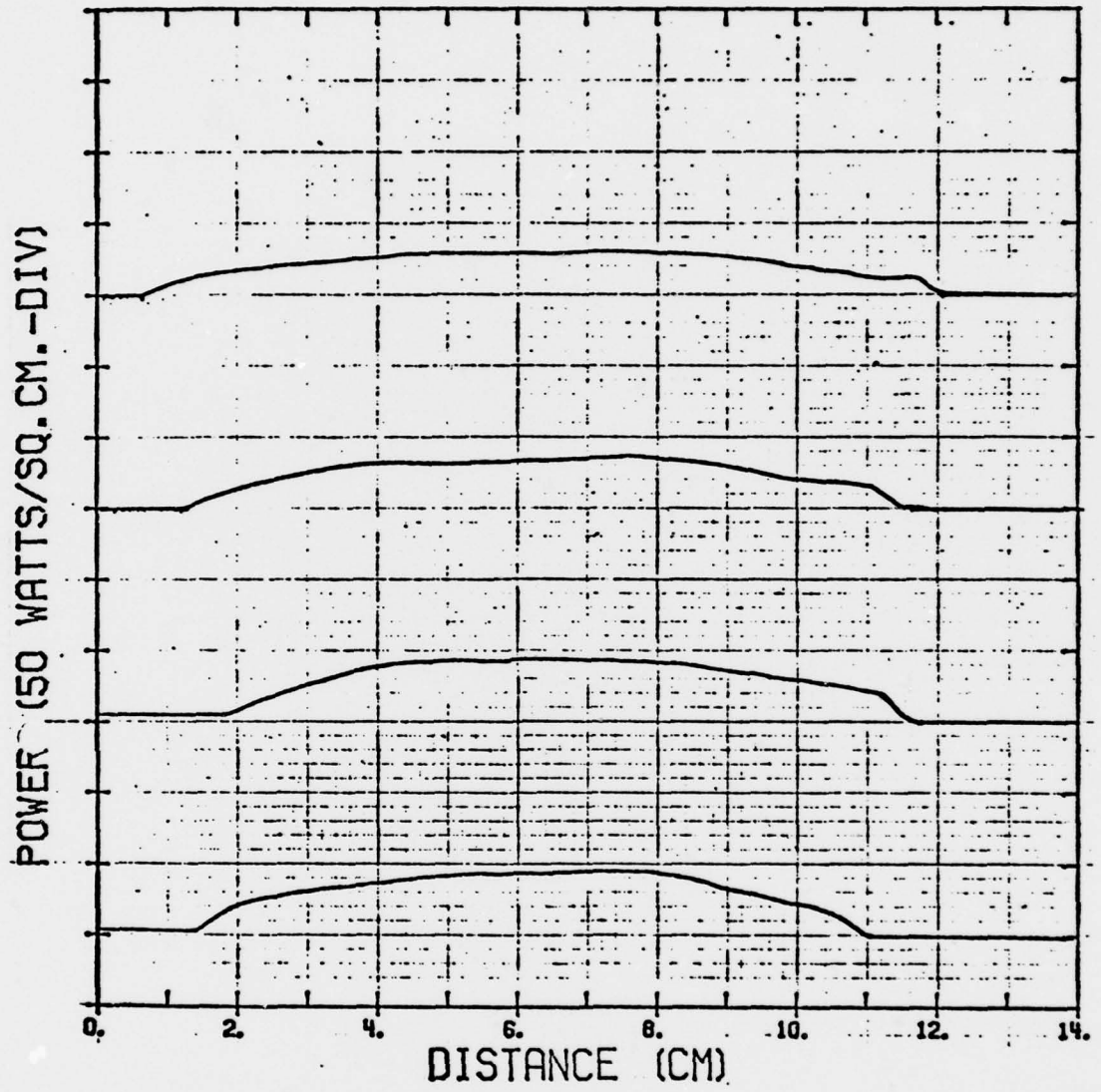

Figure B-6. Profile Set 1-5-5

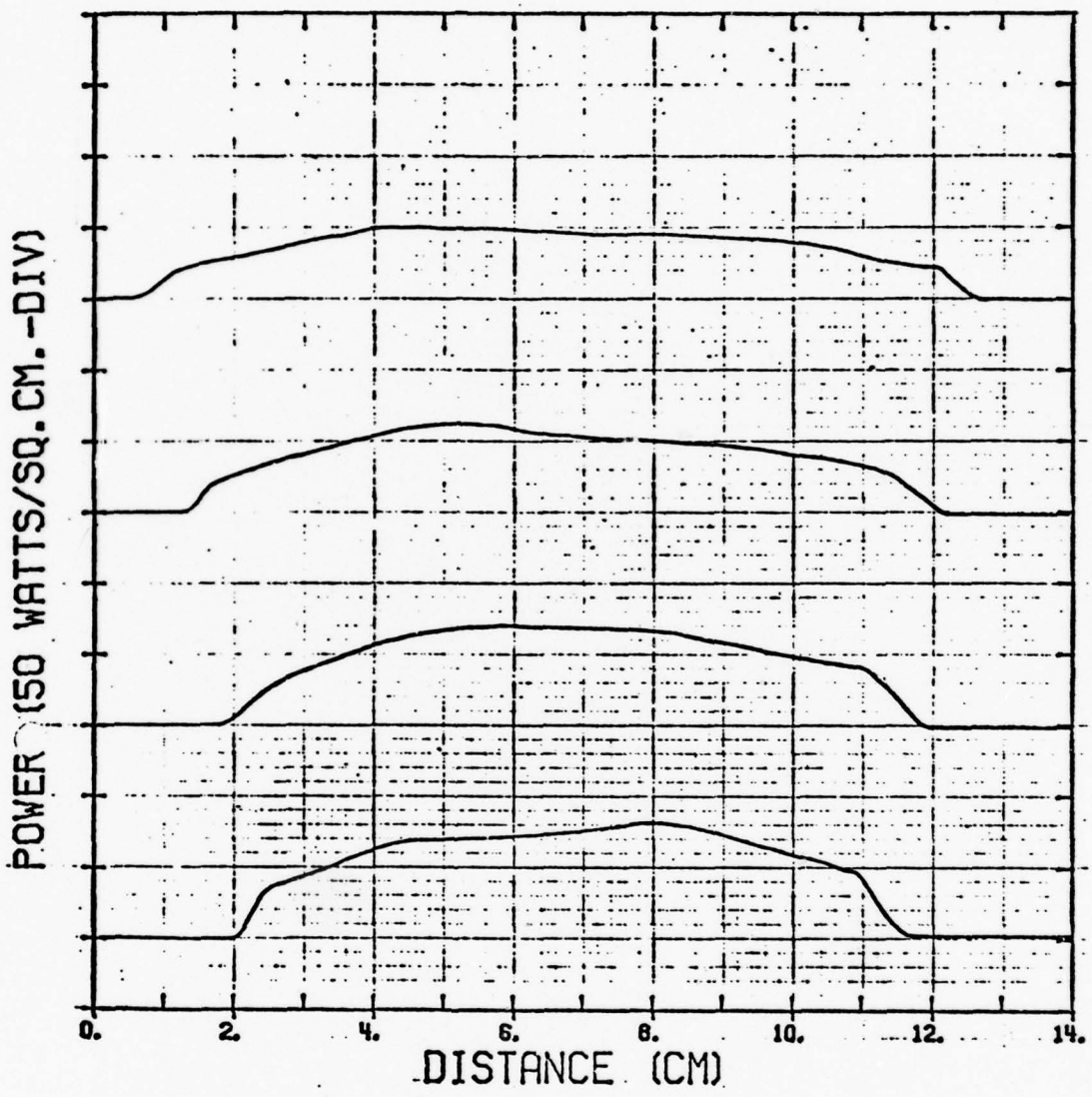

Figure B-7. Profile Set 1-8-3

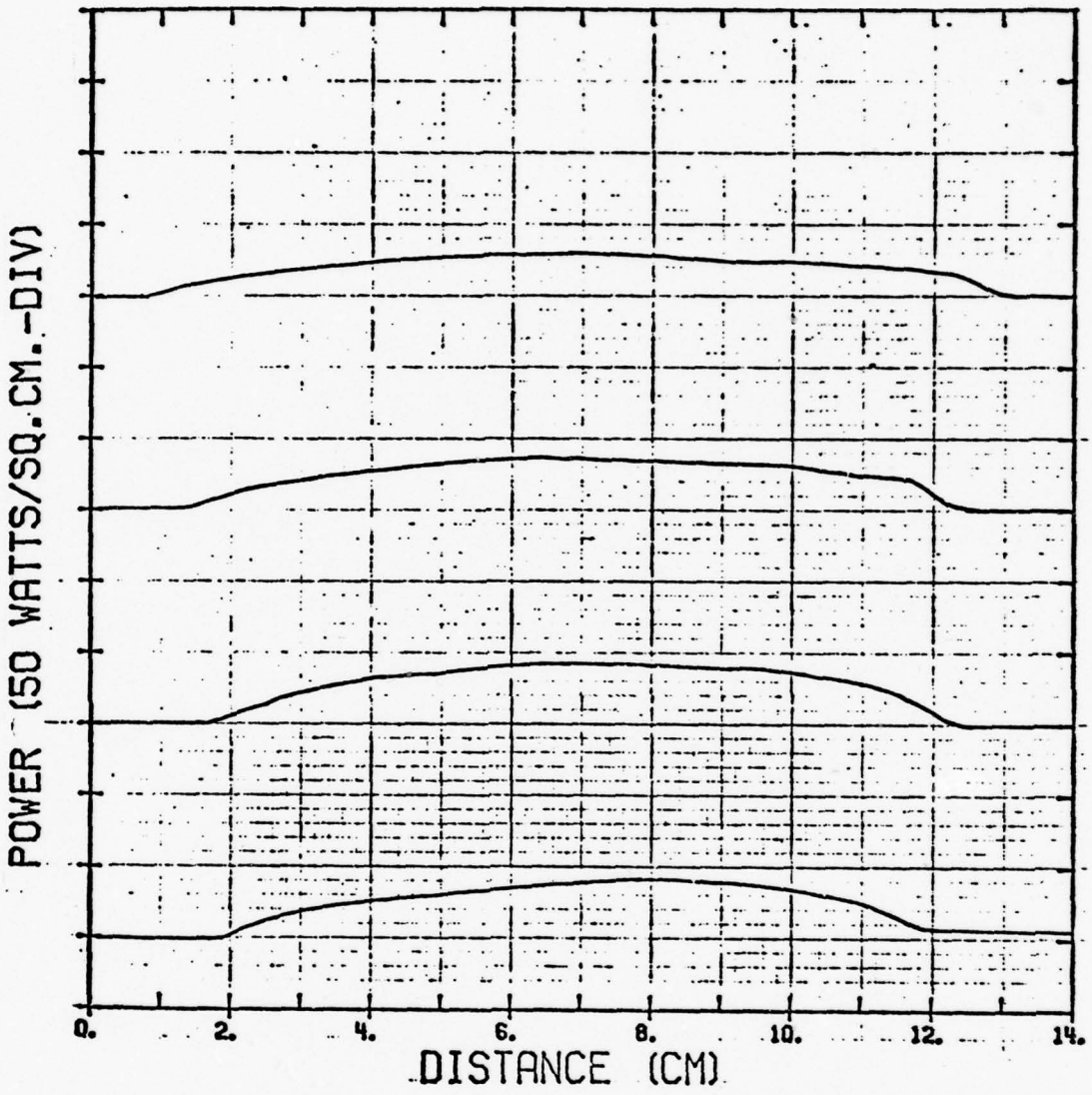

Figure B-8. Profile Set 1-8-4

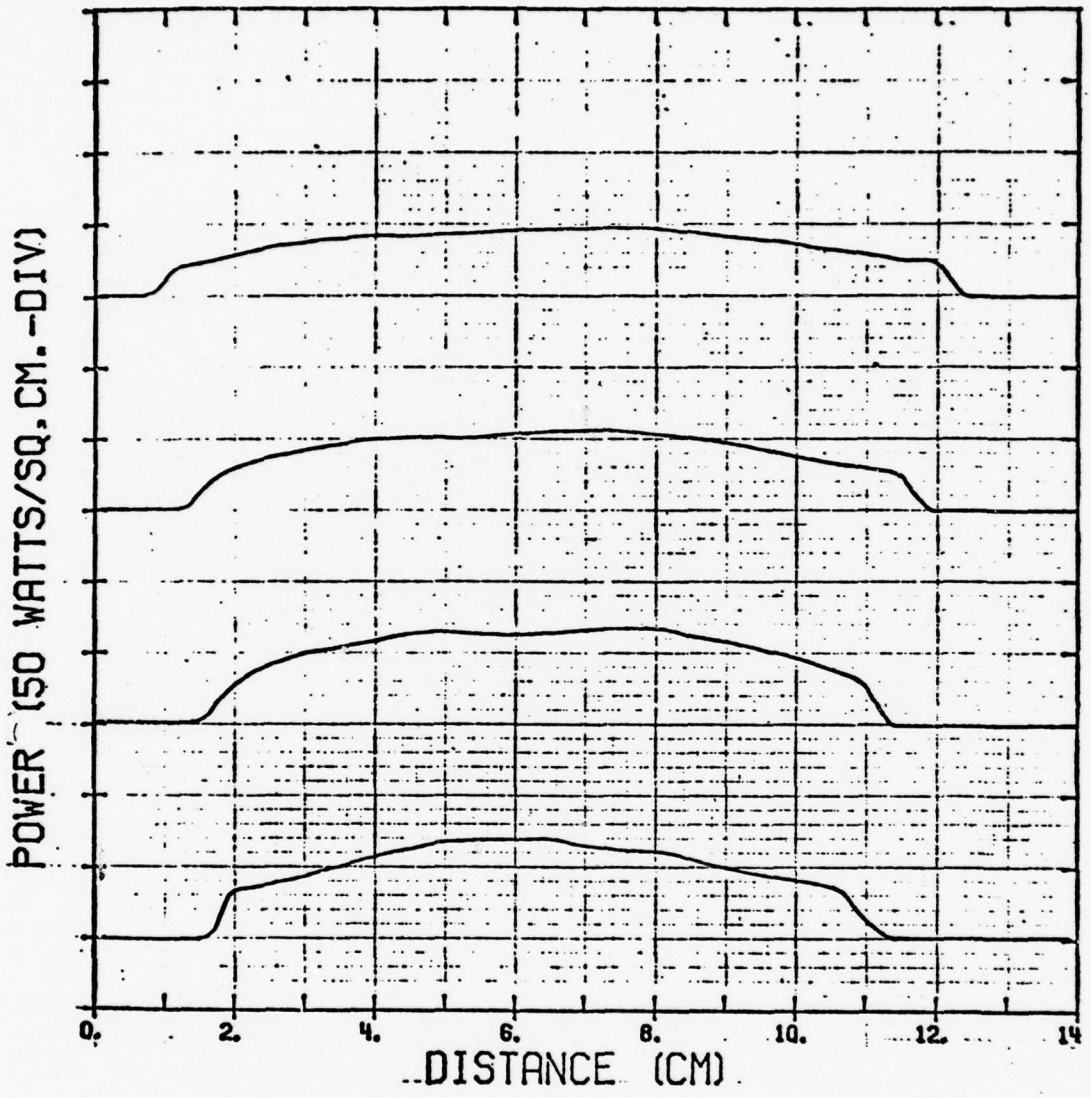

Figure B-9. Profile Set 1-8-5

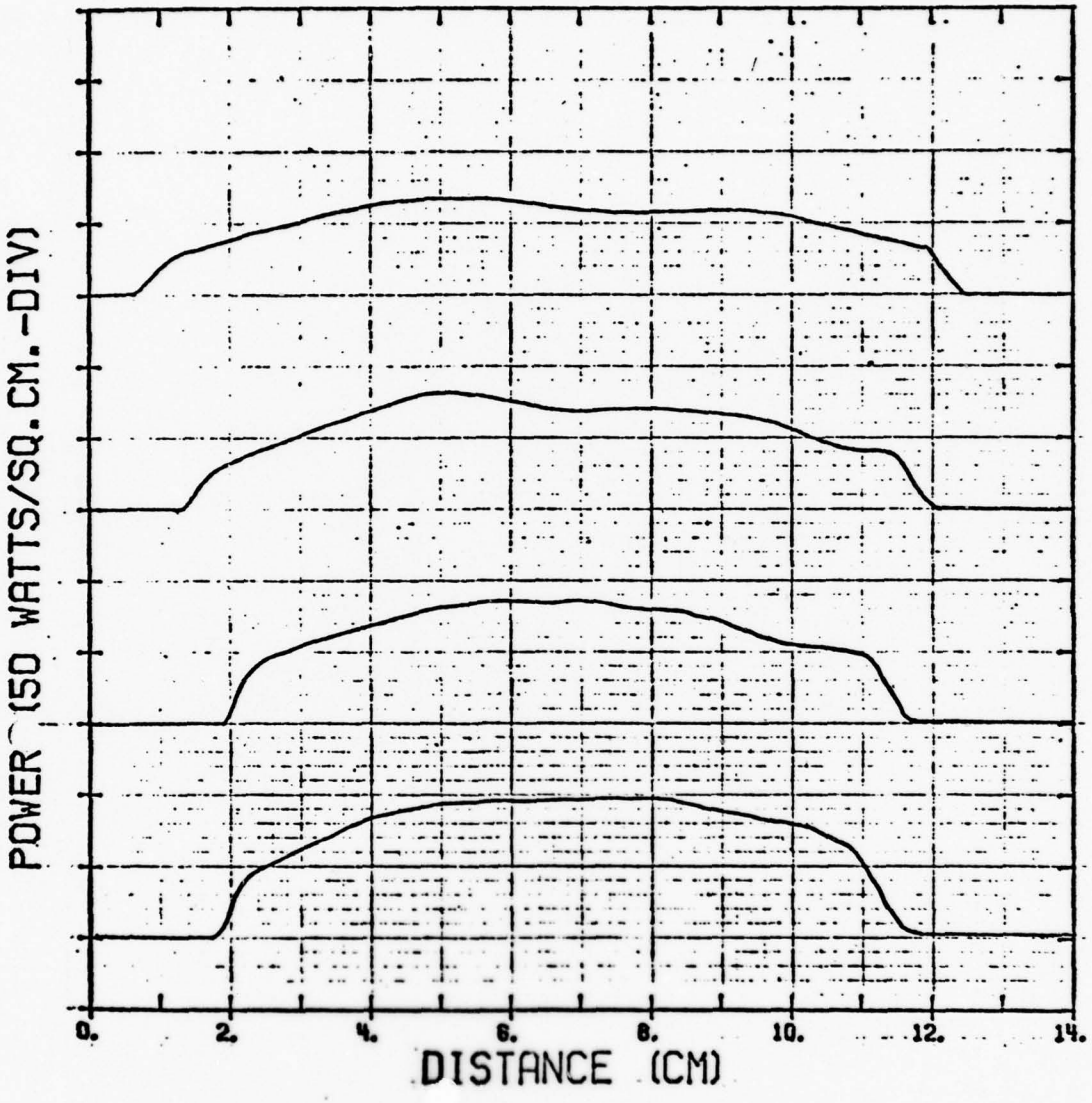

Figure B-10. Profile Set 1-10-3

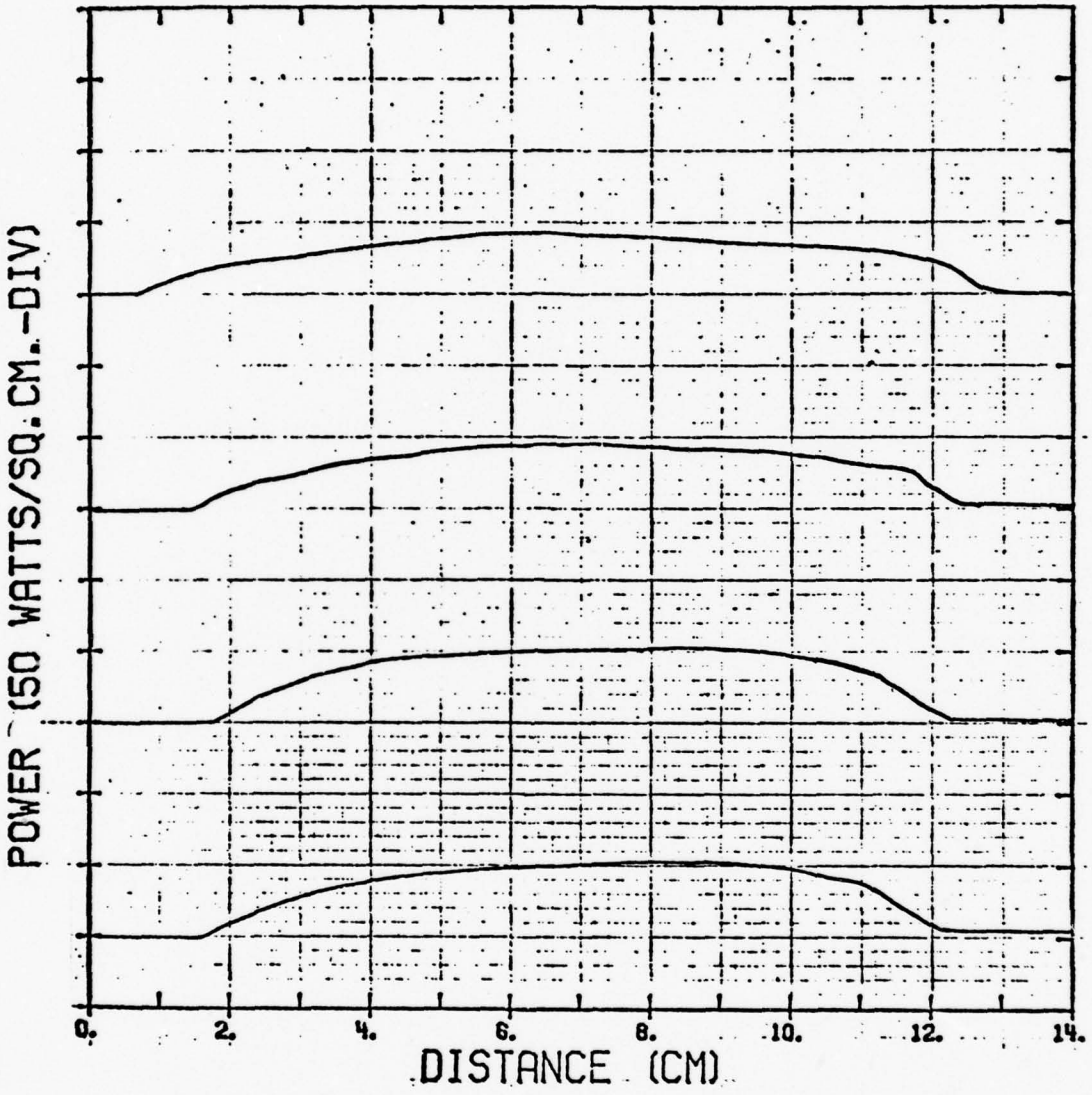

Figure B-11. Profile Set 1-10-4

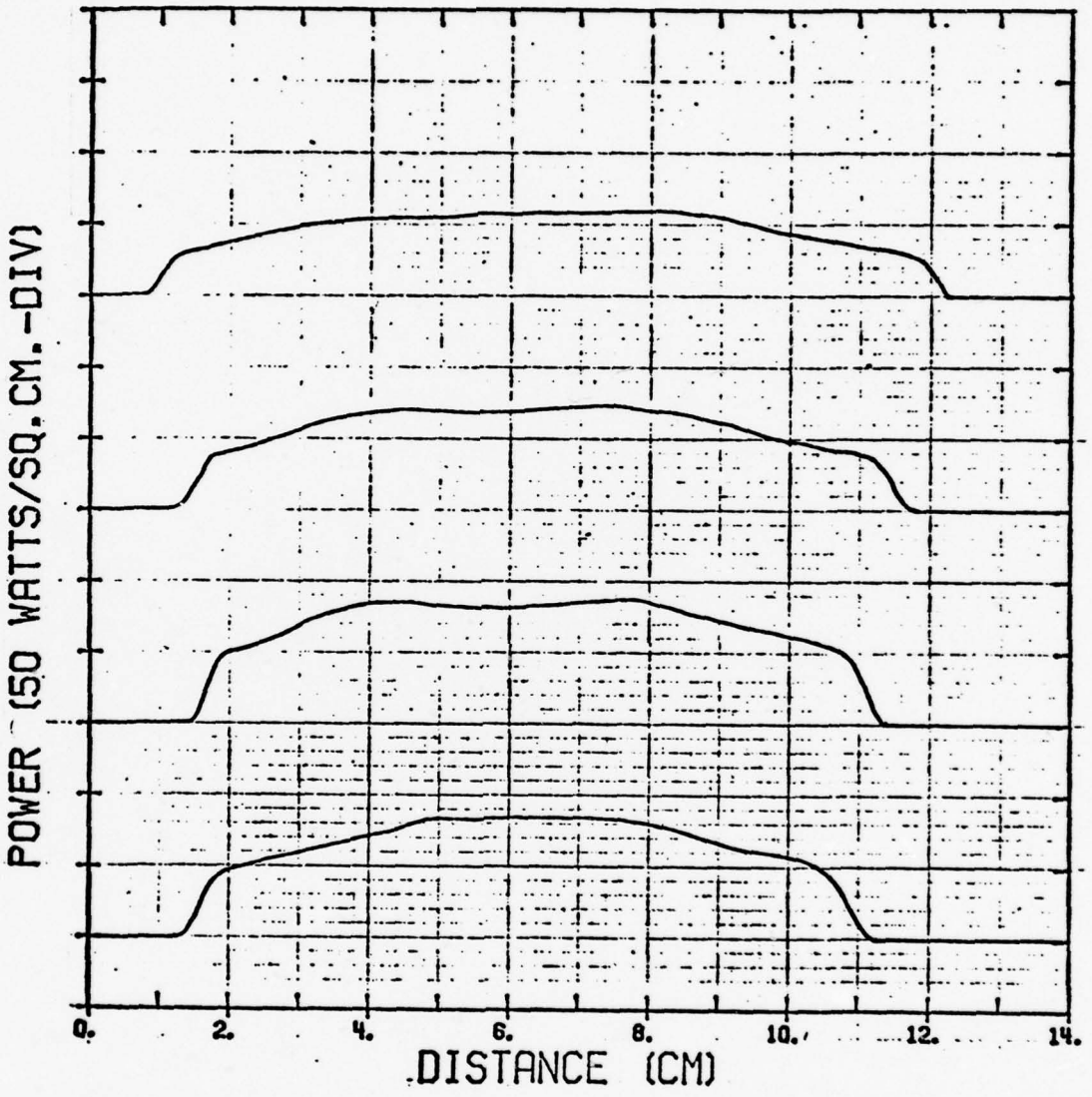

Figure B-12. Profile Set 1-10-5

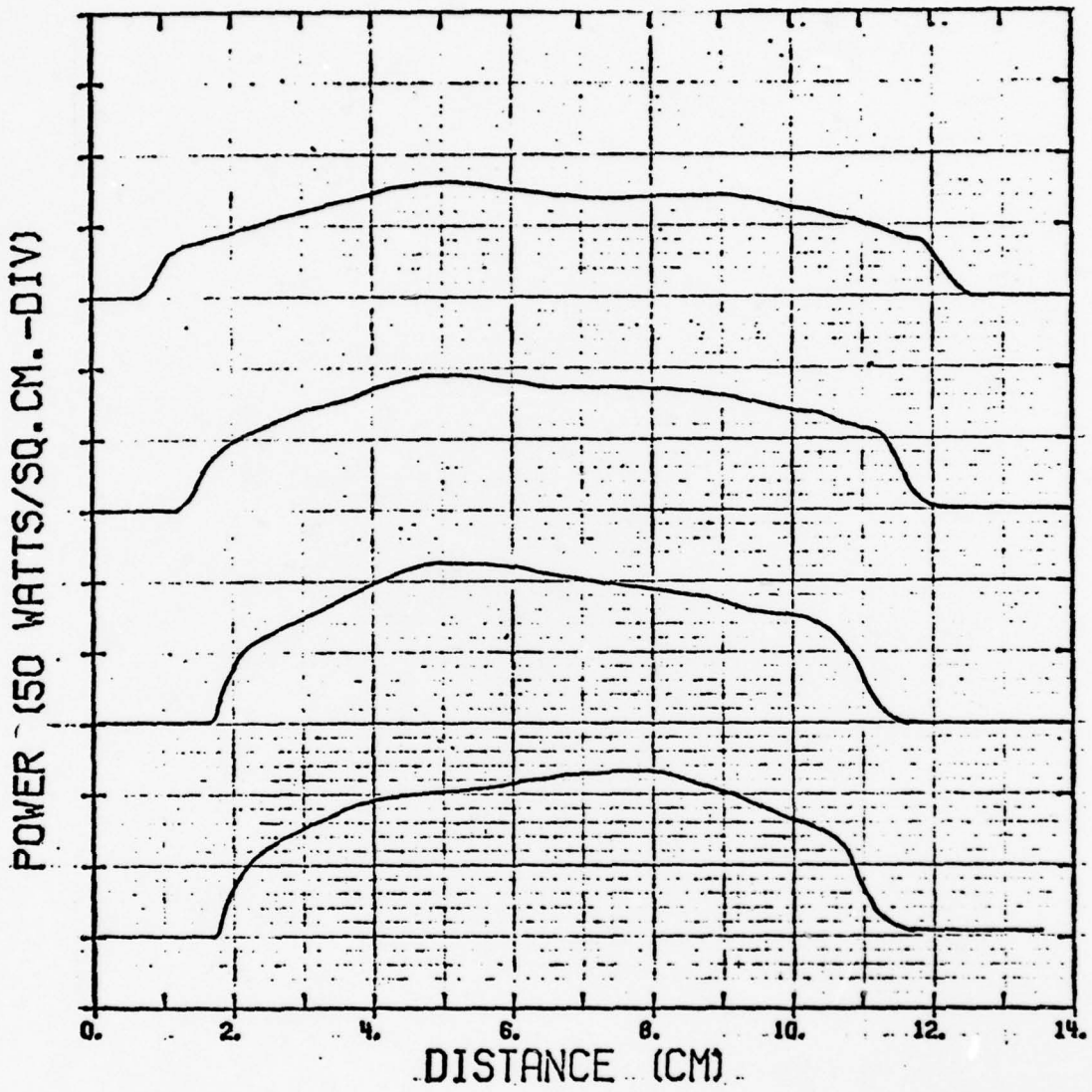

Figure B-13. Profile Set 1-12-3

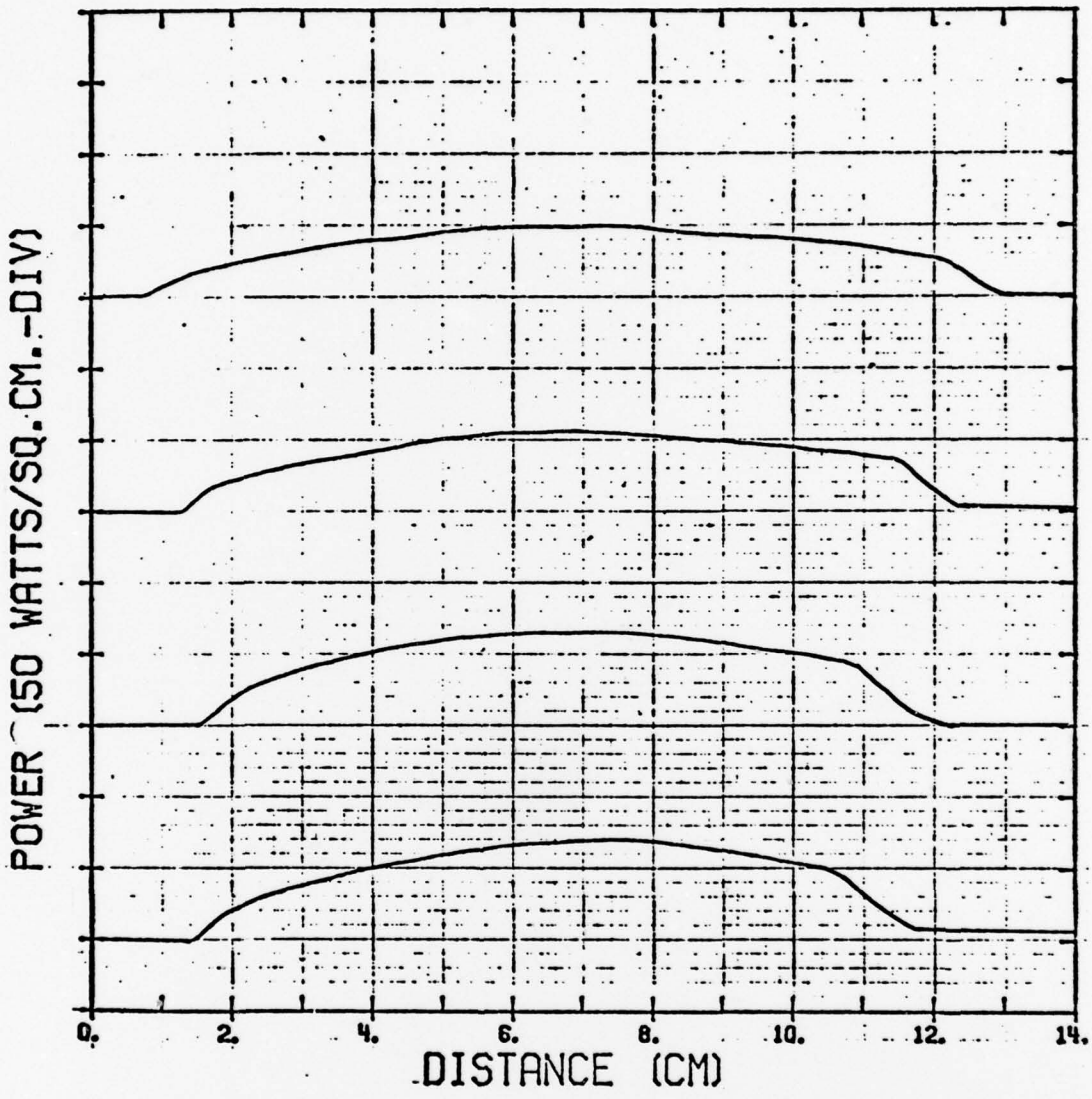

Figure B-14. Profile Set 1-12-4

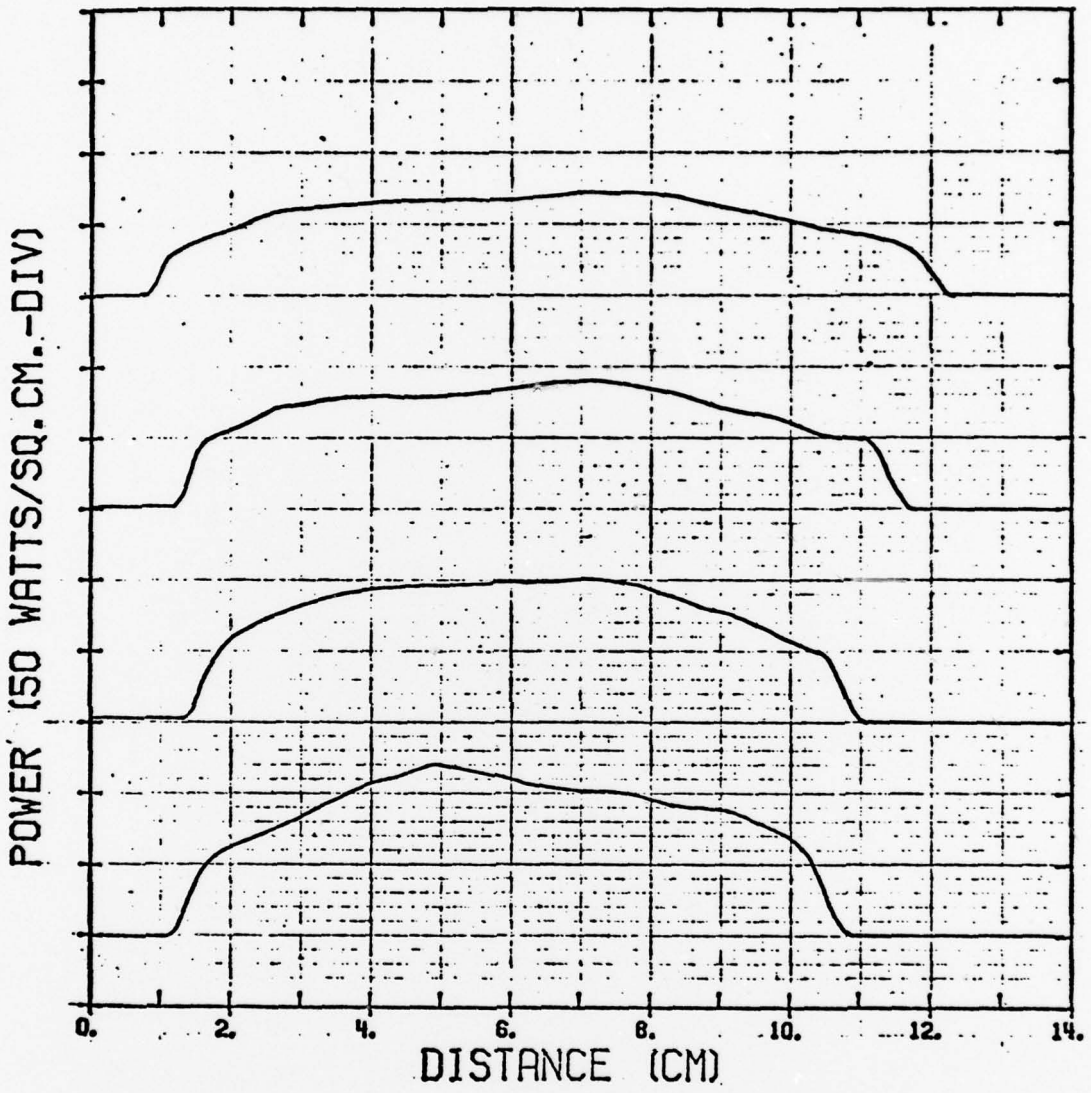

Figure B-15. Profile Set 1-12-5

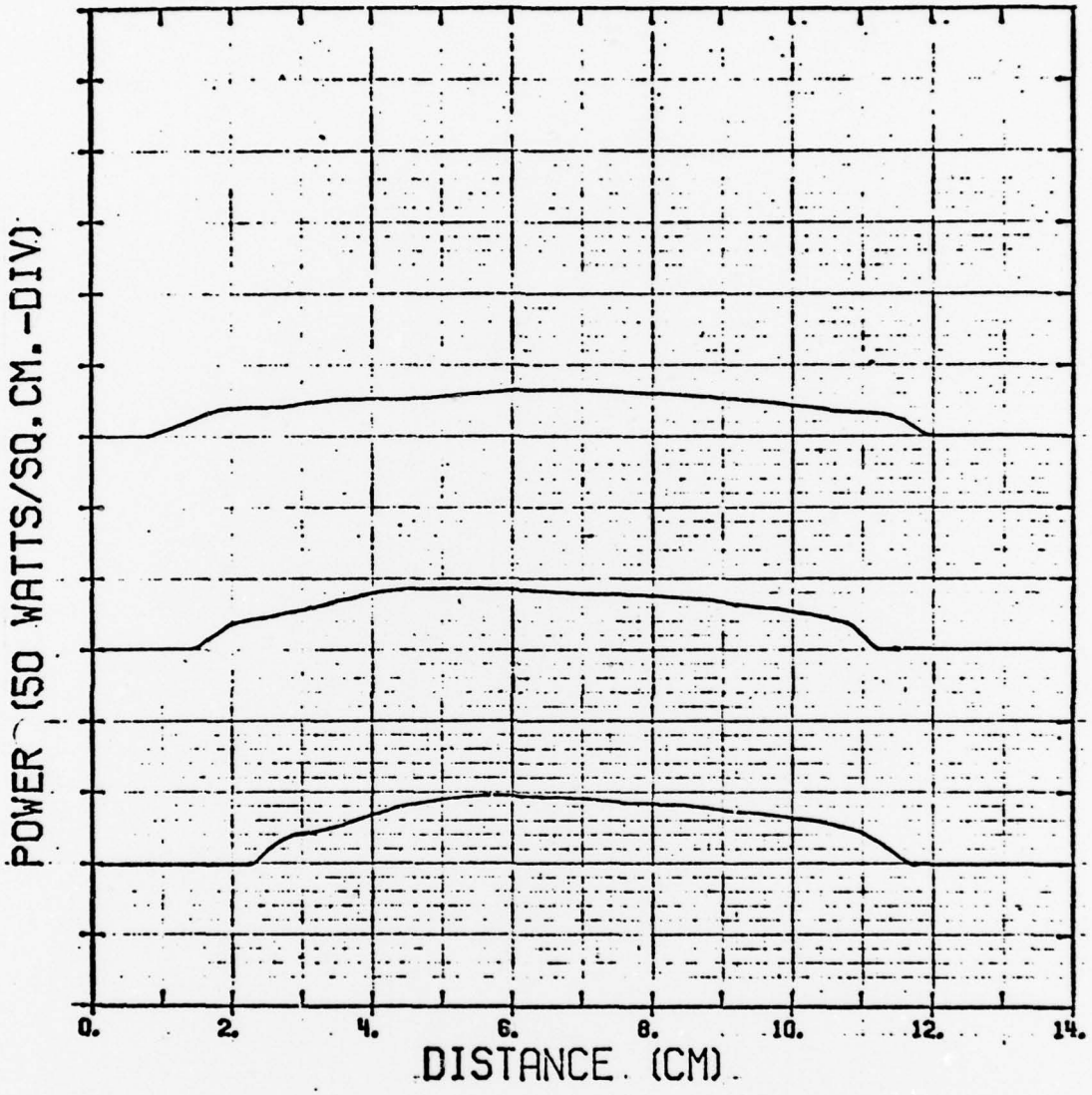

Figure B-16. Profile 2-5-3

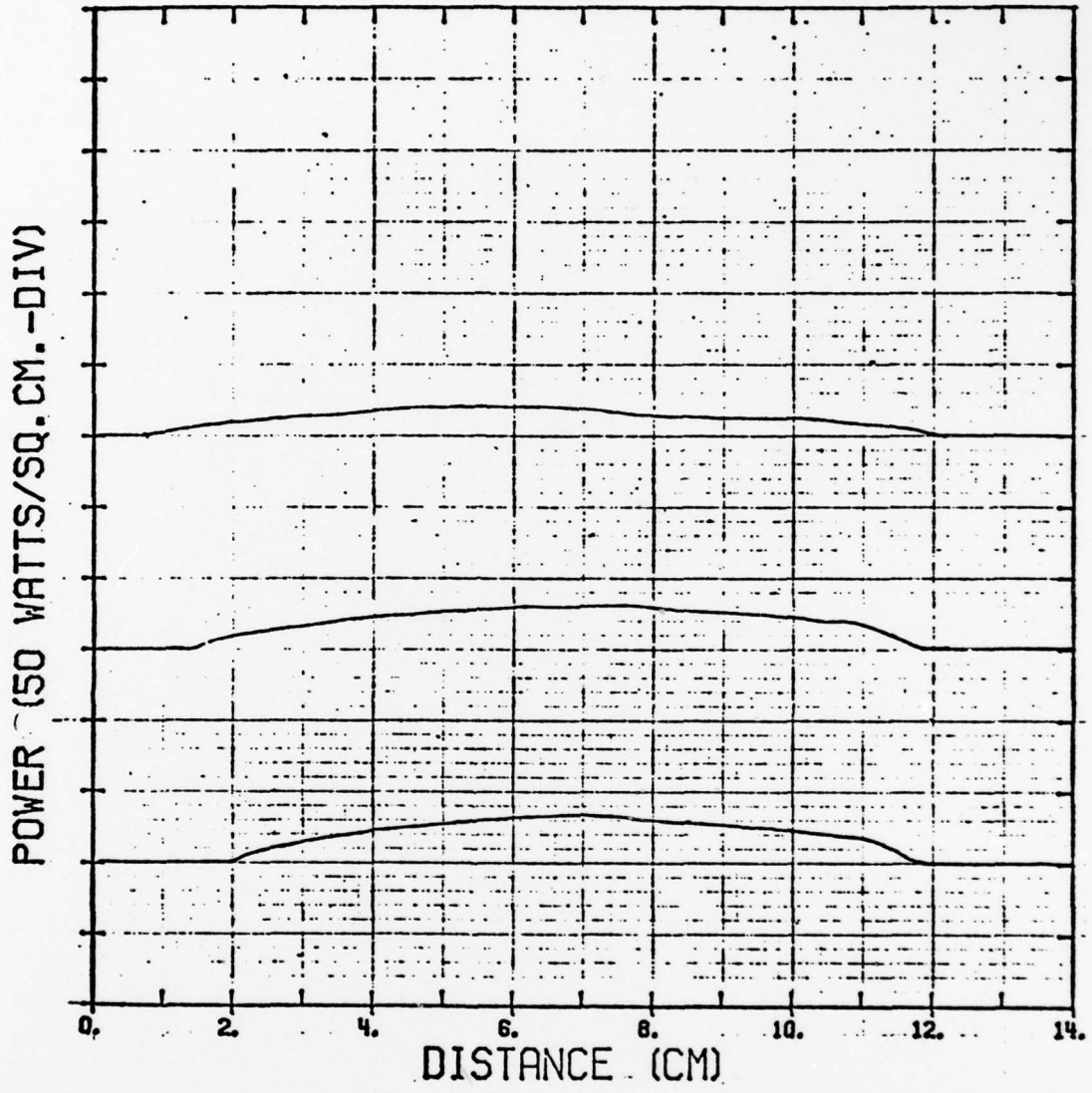

Figure B-17. Profile Set 2-5-4

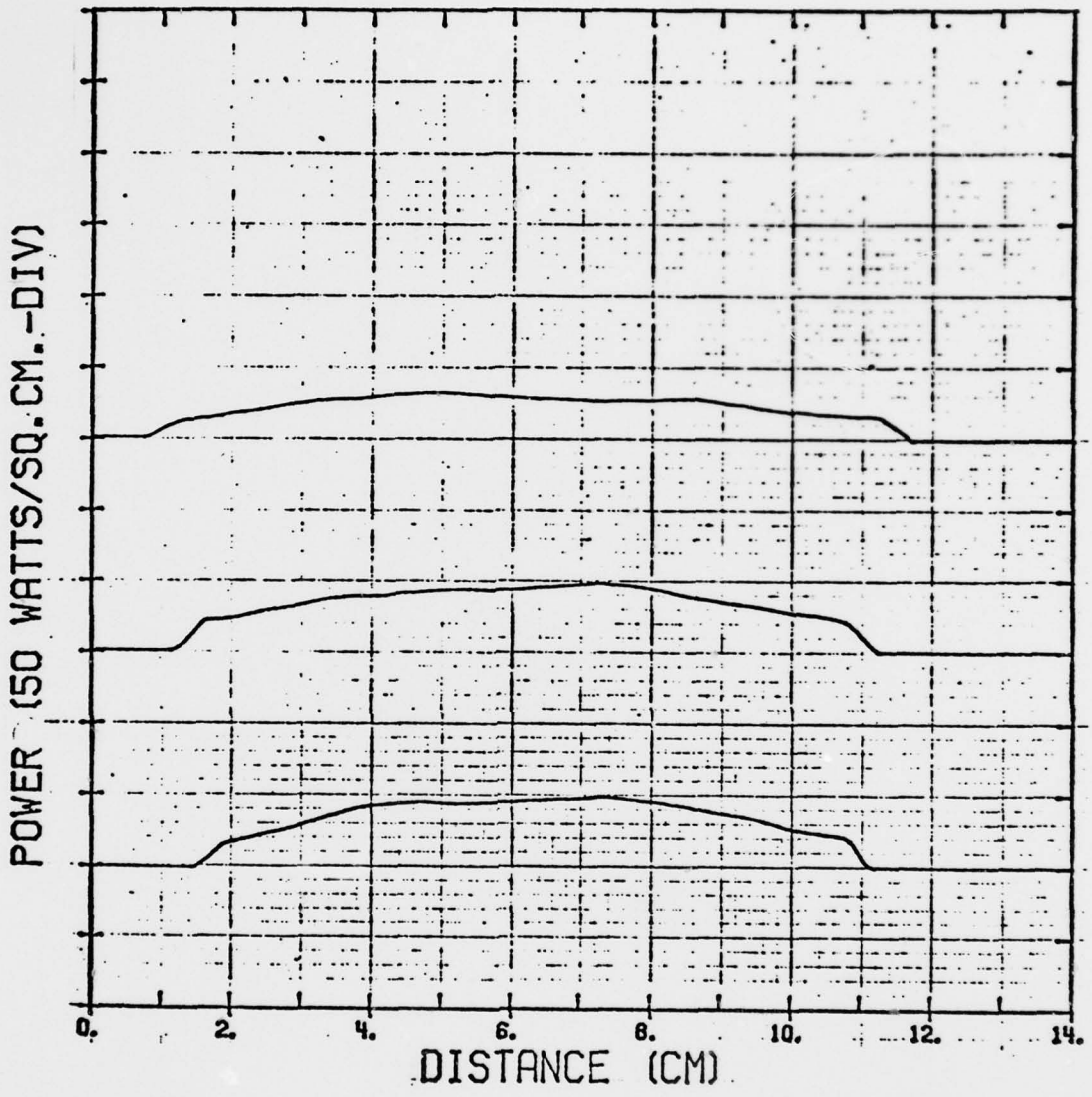

Figure B-18. Profile Set 2-5-5

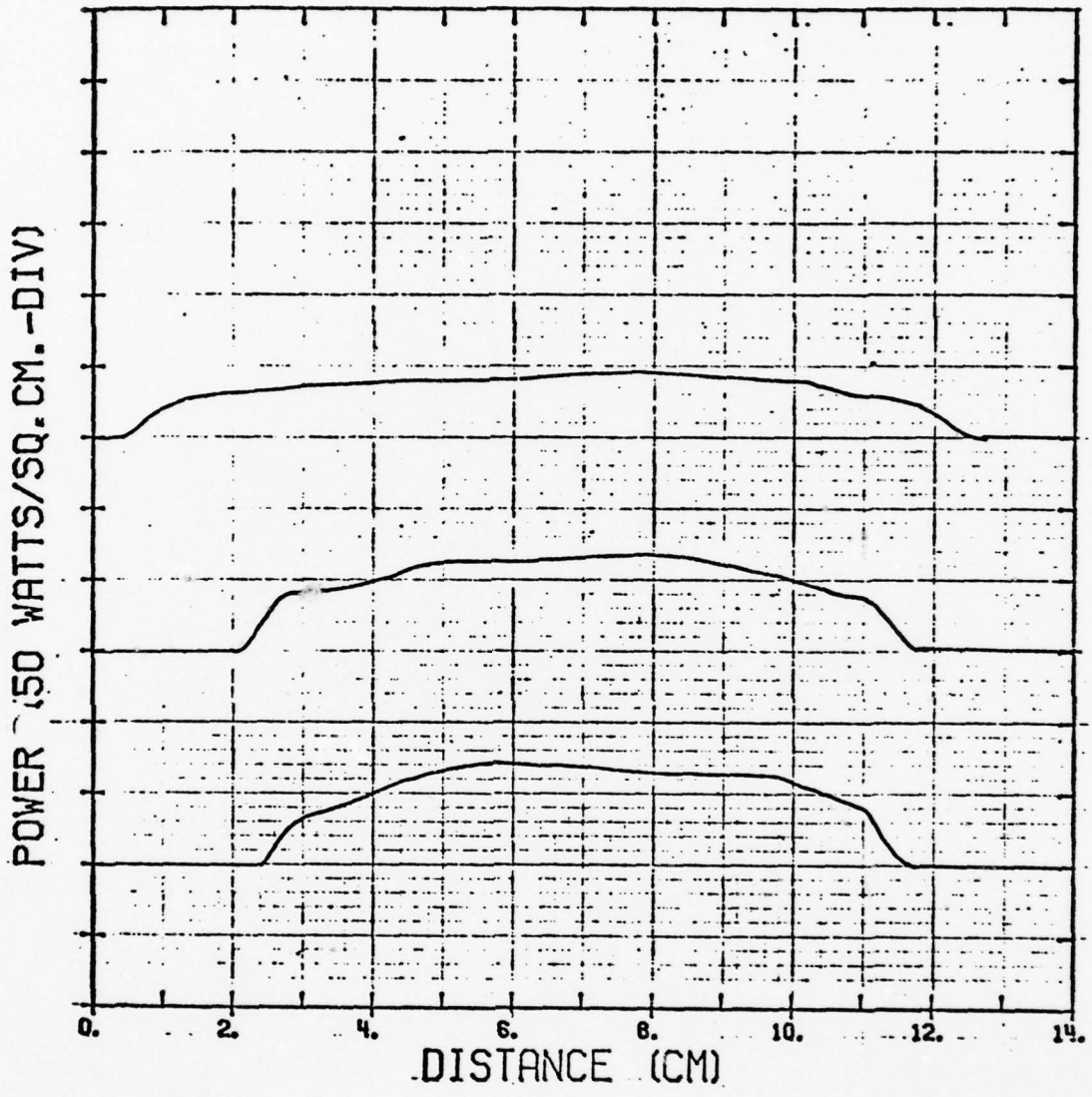

Figure B-19. Profile Set 2-8-3

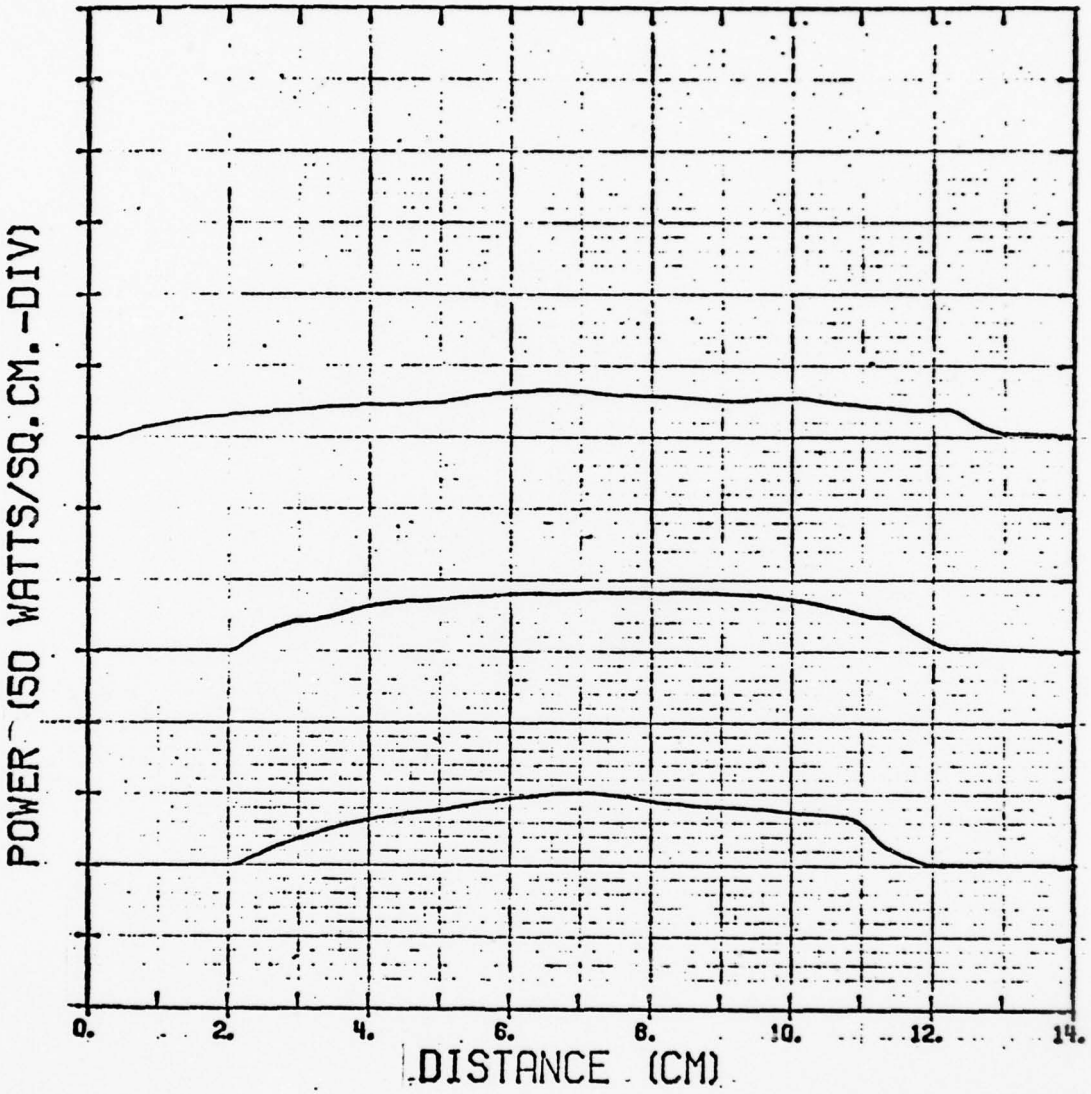

Figure B-20. Profile Set 2-8-4

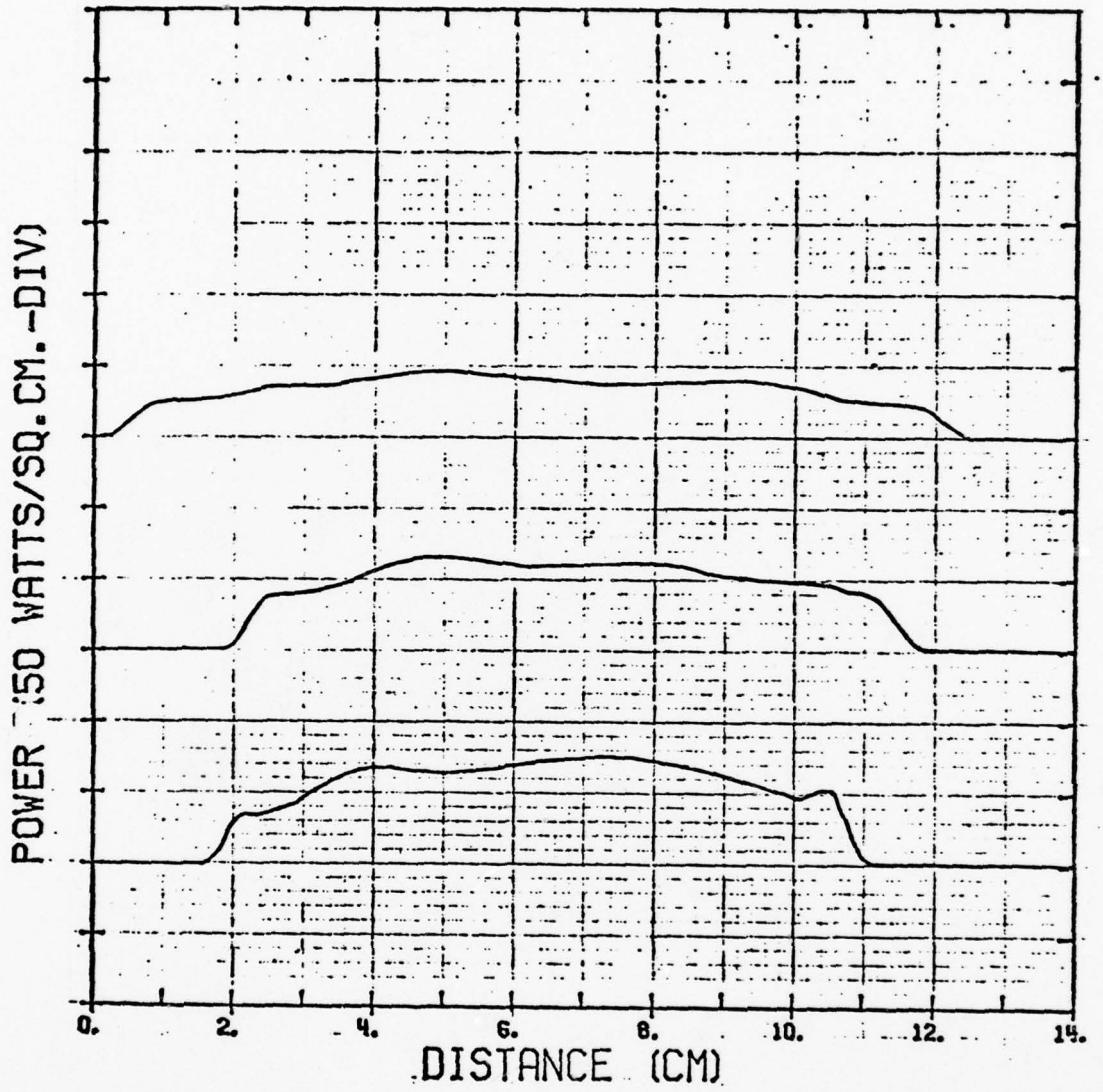

Figure B-21. Profile Set 2-8-5

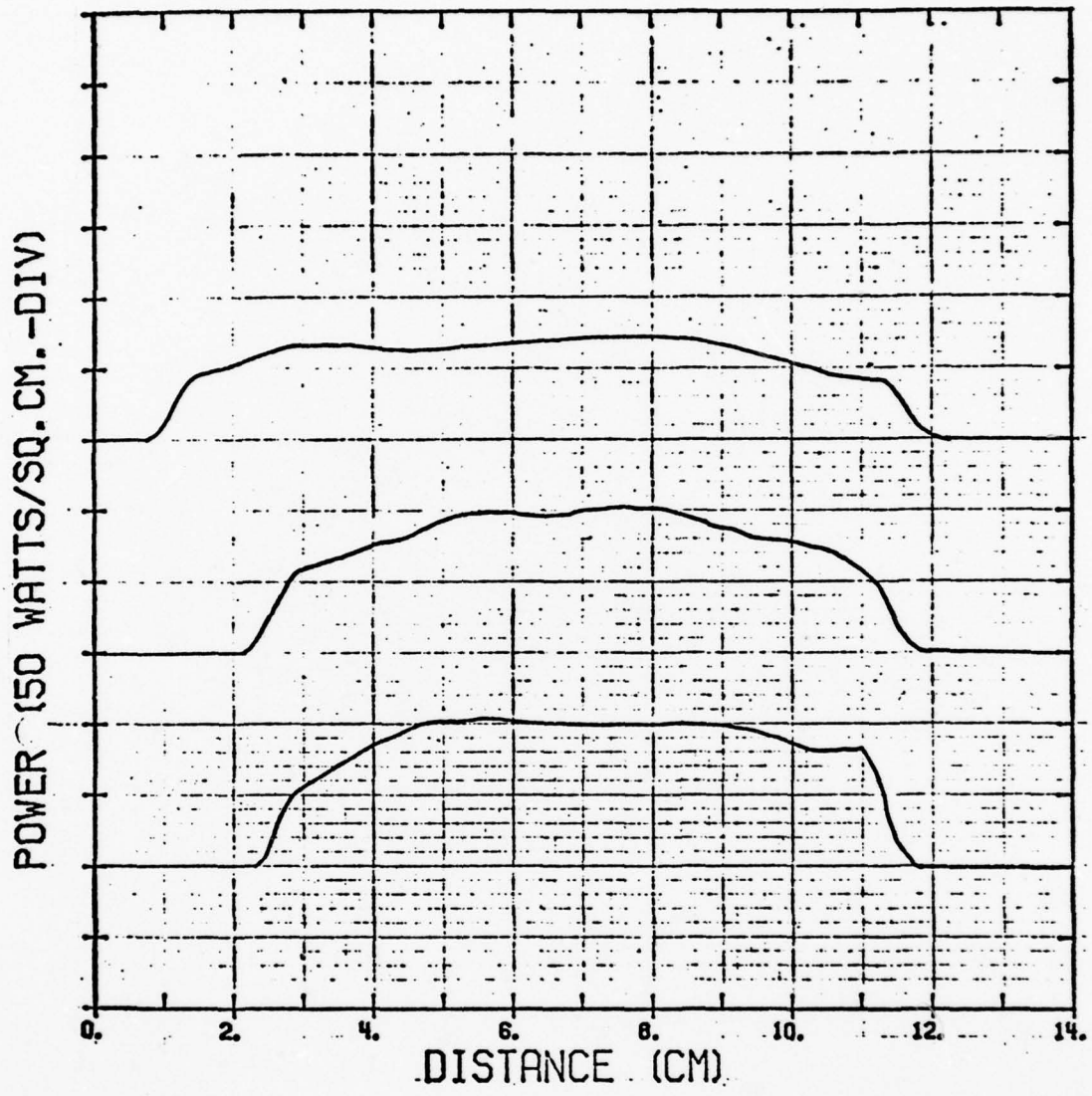

Figure B-22. Profile Set 2-12-3

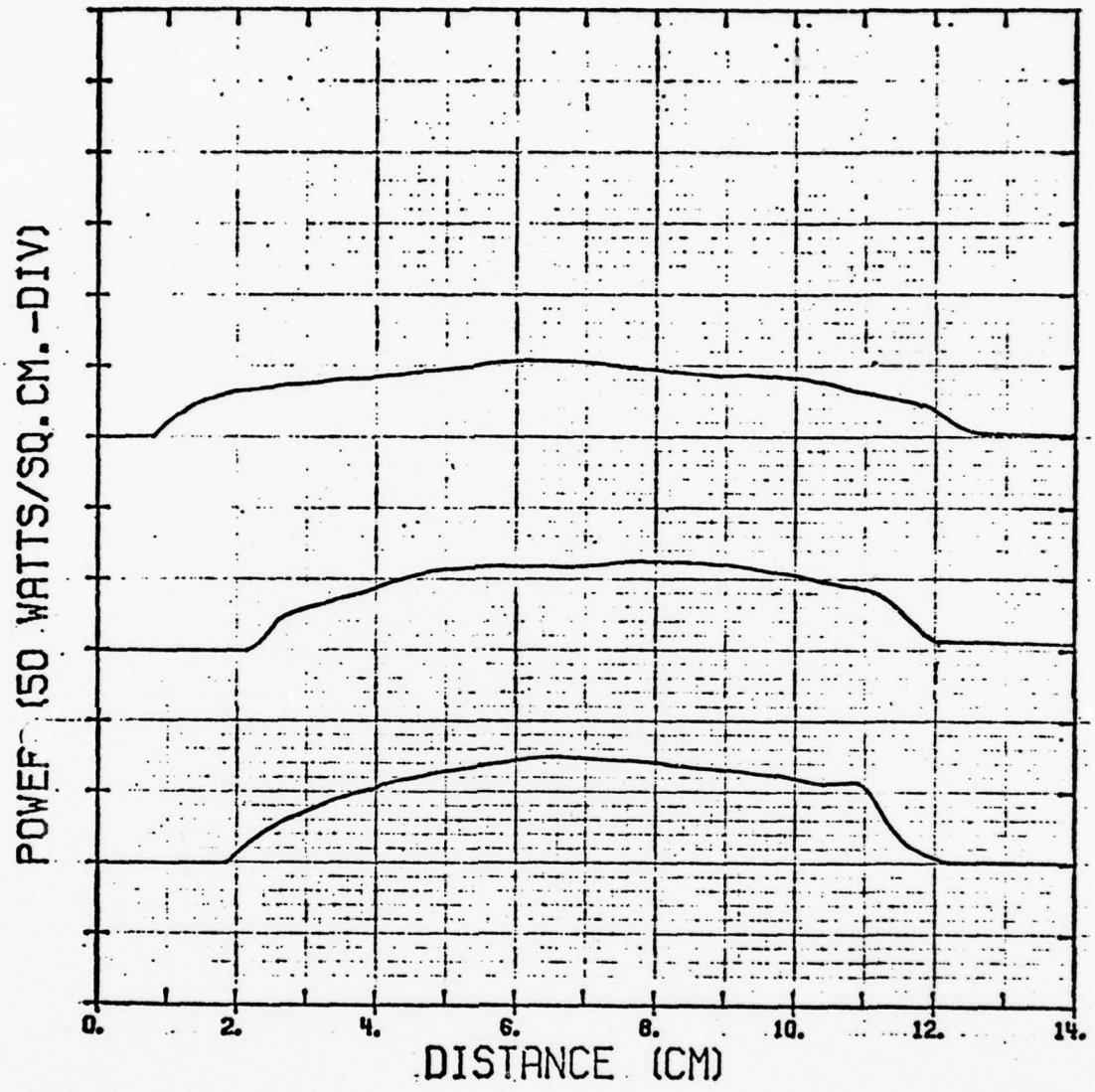

Figure B-23. Profile Set 2-12-4

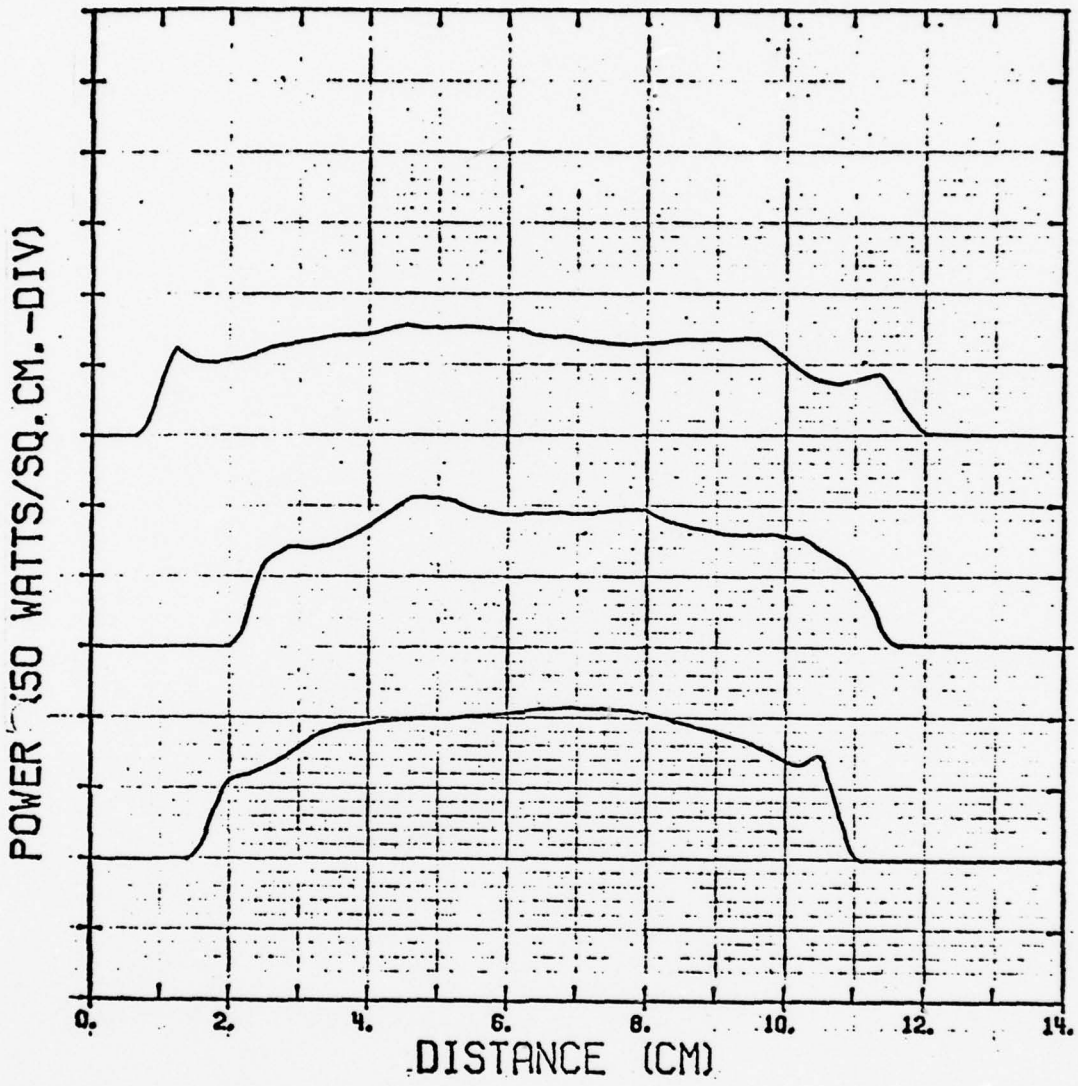

Figure B-24. Profile Set 2-12-5

Vita

Raymond Joseph Licata was born on 20 December 1946, in Detroit, Michigan. He graduated from high school in June 1965 and eventually attended Eastern Michigan University from which he received the Bachelor of Science degree in June 1969. Shortly thereafter, he joined the United States Air Force and attended Officer Training School after which he received his commission in April 1971.

His first assignment was at Warren AFB, Wyoming where he served four years as a combat crew member in missile operations. While on the job, he earned a Master of Arts degree from the University of Northern Colorado in May 1975. In 1976, he was assigned to the Foreign Technology Division at Wright-Patterson AFB, Ohio where he remained until entering the School of Engineering, Air Force Institute of Technology, in June 1977.

UNCLASSIFIED

SECURITY CLASSIFICATION OF THIS PAGE (When Data Entered)

REPORT DOCUMENTATION PAGE		READ INSTRUCTIONS BEFORE COMPLETING FORM
1. REPORT NUMBER AFIT/GEP/PH/78D-7	2. GOVT ACCESSION NO.	3. RECIPIENT'S CATALOG NUMBER
4. TITLE (and Subtitle) BEAM PROFILING OF A MULTIMODE LASER		5. TYPE OF REPORT & PERIOD COVERED MS Thesis
		6. PERFORMING ORG. REPORT NUMBER
7. AUTHOR(s) Raymond J. Licata Captain USAF		8. CONTRACT OR GRANT NUMBER(s)
9. PERFORMING ORGANIZATION NAME AND ADDRESS Air Force Institute of Technology (AFIT/EN) Wright-Patterson AFB OH 45433		10. PROGRAM ELEMENT, PROJECT, TASK AREA & WORK UNIT NUMBERS 7360-01-47
11. CONTROLLING OFFICE NAME AND ADDRESS Air Force Materials Laboratory (AFML/LPJ) Wright-Patterson AFB OH 45433		12. REPORT DATE December 1978
		13. NUMBER OF PAGES 81
14. MONITORING AGENCY NAME & ADDRESS(if different from Controlling Office)		15. SECURITY CLASS. (of this report) Unclassified
		15a. DECLASSIFICATION/DOWNGRADING SCHEDULE

16. DISTRIBUTION STATEMENT (of this Report)

Approved for public release; distribution unlimited.

17. DISTRIBUTION STATEMENT (of the abstract entered in Block 20, if different from Report)

18. SUPPLEMENTARY NOTES

Approved for public release; IAW AFR 190-17

JOSEPH P. HIPPS, Maj, USAF
Director of Information 1-23-79

19. KEY WORDS (Continue on reverse side if necessary and identify by block number)

Beam Profiling	Multimode
Beam Characteristics	"Flat Top" Profile
Swept Null Point Calorimetry	Transverse Modes
CO_2 Laser	High Power Laser

20. ABSTRACT (Continue on reverse side if necessary and identify by block number)

The experimental investigation into the intensity profile characteristics of a multimode, high-power, continuous-wave, CO_2 laser is presented. Quantitative one-dimensional profiles were obtained using an enhanced swept null point calorimeter. Qualitative two-dimensional profiles were obtained using the IR transparency material -- 3M, Type 577. The results were: ~~(1)~~ the beam divergence is 3.75 mrad; ~~(2)~~ the intensity profile is characterized basically by a circular mode pattern, but superimposed by a distinguishable rectangular component;

(Continued on Reverse)

DD FORM 1 JAN 73 1473 EDITION OF 1 NOV 65 IS OBSOLETE

UNCLASSIFIED

next page

SECURITY CLASSIFICATION OF THIS PAGE (When Data Entered)

(3) the rectangular component only varies in intensity proportional to the laser power and inversely proportional to the optical path length; ~~(4)~~ the shot stability is about ±7 w/cm^2; and, ~~(5)~~ the average profile deviation from an idealized 'flat top' profile varies from 11 to 15%.

+ or - Sq. Cm.